Salvia miltiorrhiza polysaccharide and its related metabolite 5-methoxyindole-3-carboxaldehyde ameliorate experimental colitis by regulating Nrf2/Keap1 signaling pathway

Yu-Ping Fu [a,b,c,1], Xi Peng [a,1], Chao-Wen Zhang [a,1], Quan-Xing Jiang [a], Cen-Yu Li [a], Berit Smestad Paulsen [c], Frode Rise [d], Chao Huang[b], Bin Feng[e], Li-Xia Li[a], Xing-Fu Chen[f], Ren-Yong Jia[b], Yang-Ping Li [g], Xing-Hong Zhao [a], Gang Ye [a], Hua-Qiao Tang [a], Xiao-Xia Liang[a], Cheng Lv [a], Meng-Liang Tian[f], Zhong-Qiong Yin [a], Yuan-Feng Zou [a, b,1*]

[a] Natural Medicine Research Center, College of Veterinary Medicine, Sichuan Agricultural University, Chengdu 611130, China;

[b] Key Laboratory of Animal Disease and Human Health of Sichuan Province, College of Veterinary Medicine, Sichuan Agricultural University, Chengdu 611130, China

[c] Section for Pharmaceutical Chemistry, Department of Pharmacy, University of Oslo, P.O. Box 1068, Blindern, 0316 Oslo, Norway

[d] Department of Chemistry, University of Oslo, P.O. Box 1033, Blindern, 0315 Oslo, Norway

[e] Animal Nutrition Institute, Sichuan Agricultural University, Chengdu 611130, China

[f] Key Laboratory of Crop Ecophysiology and Farming System in Southwest China, Ministry of Agriculture, College of Agronomy, Sichuan Agricultural University, Chengdu 611130, China

[g] State Key Laboratory of Crop Gene Exploration and Utilization in Southwest China, College of Agronomy, Sichuan Agricultural University, Chengdu, 611130 China

[1] These authors contributed equally to this work.

*Corresponding authors: Y.-F. Zou, Email address: yuanfengzou@sicau.edu.cn (Y.-F. Zou).

Abstract: The roots of *Salvia miltiorrhiza* have been used in Traditional Chinese Medicine for thousands of years. However, tons of aerial parts of this plant are usually discarded in the production of roots preparation. To make better use of these plant resources, the polysaccharide isolated from the aerial part of *S. miltiorrhiza* was investigated for its potential protection against intestinal diseases. A pectic polysaccharide (SMAP-1) was isolated and characterized being composed of homogalacturonan as the main chain and rhamnogalacturonan type I as ramified region, with side chains including arabinans and possible arabinogalactan type I and II. SMAP-1 exhibited robust protective effects against dextran sodium sulfate (DSS)-induced colitis and restored colitis symptoms, colonic inflammation, and barrier functions. Anti-oxidative effects were also observed by up-regulating Nrf2/Keap1 signaling pathway. Additionally, the level of serum 5-methoxyindole-3-carboxaldehyde (5-MC) was restored by SMAP-1 identified in metabolomic analysis, being correlated with the aforementioned effects. Protection against oxidative stress on intestinal porcine enterocyte cells (IPEC-J2) by 5-MC was observed through the activation of Nrf2/Keap1 system, as also shown by SMAP-1. In conclusion, SMAP-1 could be a promising candidate for colitis prevention, and 5-MC could be the signal metabolite of SMAP-1 in protecting against oxidative stress in the intestine.

Keywords: *Salvia miltiorrhiza*; pectic polysaccharide; antioxidant activity; experimental colitis; metabolomic analysis; 5-methoxyindole-3-carboxaldehyde

1 Introduction

Inflammatory bowel disease (IBD) is a non-specific, chronic, and recurrent inflammatory disease of the intestinal tract including ulcerative colitis (UC) and Crohn's disease (CD) (Bernstein et al., 2010; Lee, Kwon, & Cho, 2018). It causes lesions in the colon, rectum, and colonic mucosa, as well as depression, weight loss, loose and bloody stools in severely sick patients (Luo, Shu, & Chen, 2019; Mehta, Lindsay, & Silver, 2013). The causes of IBD remain unclear, but research has progressed to reveal the pathogenesis of this disease, which includes genetic factors, gut microbiota, environmental factors, immunological abnormalities, and immune system dysregulation (Guan, 2019). Additionally, recent studies have shown that oxidative stress, an imbalance between the production and elimination of reactive oxygen species (ROS), is a key factor in the pathophysiology and progression of IBD, and is related to inflammation of the intestinal mucosa due to cellular and molecular damage caused by the excessive production of ROS (Bourgonje et al., 2020). Therefore, defending against oxidative stress, such as eliminating ROS and promoting antioxidant enzyme activities, is an effective way to prevent IBD (Bourgonje et al., 2020; Hwang et al., 2020). The application of antioxidant therapy in the treatment of UC has also been shown to be an effective approach in clinical trials (Tahvilian et al., 2021).

The nuclear transcription factor erythroid 2–related factor 2 (Nrf2) has been shown to play an important role in reducing intestinal mucosal injury by controlling ROS, inhibiting inflammation, and regulating intestinal permeability (Wen et al., 2019). Under stress conditions, Nrf2 is released from Kelch-like ECH associated protein 1 (Keap 1, an adaptor protein of Cul3 E3 ubiquitin ligase) to migrate from the cytoplasm to the nucleus, thereby activates a series of gene expressions of antioxidant response elements (ARE)-dependent antioxidative and cytoprotective proteins, such as heme oxygenase (HO-1), quinone oxidoreductase 1 (NQO1) and glutathione oxidase (GSH-PX) (Tu, Wang, Li, Liu, & Sha, 2019; Wen et al., 2019). Therefore, the regulation of

Nrf2/Keap1 signaling pathway offers new perspectives for the treatment of IBD, especially UC (Piotrowska, Swierczynski, Fichna, & Piechota-Polanczyk, 2021).

The dried root of *Salvia miltiorrhiza* is a traditional Chinese herbal medicine used to promote blood circulation (Hao, Ge, & Xiao, 2018), eliminate static blood (Wang et al., 2018), dredge meridians, and treat coronary heart disease (Li, Zhong, & Moses, 2005; Li, Xu, & Liu, 2018). However, the aerial parts of *S. miltiorrhiza* are always discarded when the roots are collected. These aerial parts have been shown to contain similar bioactive components as the roots, such as salvianolic acid, polysaccharides, flavonoids, and triterpenes, and to exhibit similar pharmacological activities, such as anti-oxidation and curative effects on cardiovascular diseases and diabetes (Yang, Wi, & Zhang, 2020). The anti-oxidative effects of the aerial parts of *S. miltiorrhiza* have been shown to be related to ameliorating diabetic nephropathy (Xiang, 2019), regulating glycolipid metabolism (Yu et al., 2018), anti-Alzheimer (Chen, Hu, Zhang, Han, & Li, 2018), protecting the cardiovascular system, and restoring the intestinal barrier and microbiota composition in diabetic mice (Yang et al., 2020). Polysaccharide is one of the bioactive compounds identified in the roots of *S. miltiorrhiza* (Jiang et al., 2020; X. Wang et al., 2019; Zhao et al., 2020). However, few studies have been performed on the polysaccharides from the aerial parts, such as isolation, structural characterization, or pharmacological properties. Recently, it has been reported that natural plant polysaccharides are beneficial for intestinal health as indigestible biopolymers with no obvious side effects, and thus have drawn increasing attention to their pharmacological functions in IBD compared with other drug treatments with potential immune inhibition after long-term use (Yang, Zhao, Li, Guo, & Gao, 2022). A variety of polysaccharides with anti-oxidative effects have been isolated from the leaves of medicinal plants (Ahmad et al., 2022; Huang et al., 2021). Based on the promising anti-oxidative properties of the aerial part of *S. miltiorrhiza*, we hypothesized that the polysaccharide isolated from these aerial parts could be a potential anti-oxidant

substance and play a role in the treatment of UC. It would also be beneficial for expanding the application of these unutilized plant materials.

Thus, this study aimed to isolate and purify a polysaccharide from the aerial parts of *S. miltiorrhiza,* and to investigate its structural characteristics. Its protective effect against the experimental UC mice with focusing on anti-oxidative properties would also be studied. Metabolomic analysis would be performed to investigate the potential biomarker for this polysaccharide on the effects of UC.

2 Materials and methods

2.1 Materials and reagents

The aerial parts of *Salvia miltiorrhiza* were collected from Jiqing Town, Zhongjiang County, Deyang City, Sichuan Province, China, on 10th October 2019. Fresh aerial parts of *S. miltiorrhiza* were cleaned, dried in an air oven at 40 ℃, and ground into powder. A voucher specimen No. 20191101 is deposited at the Department of Pharmacy, College of Veterinary Medicine, Sichuan Agricultural University, China. The intestinal porcine enterocyte cell line (IPEC-J2) was obtained from Shanghai Institutes of Biological Sciences, Chinese Academy of Sciences (Shanghai, China). Dextran sodium sulfate (DSS, 36 000–50 000 Da) was purchased from Sigma-Aldrich (USA). 5-Methoxyindole-3-carboxaldehyde was purchased from Shanghai yuanye Bio-Technology Co, Ltd. All other chemical reagents were of analytical grade.

2.2 Extraction and isolation of polysaccharide fractions

The extraction and isolation of polysaccharides were carried out according to the methods reported earlier (Huang et al., 2021). Briefly, the aerial parts of *S. miltiorrhiza* were pre-extracted with 80% ethanol (V/V) to remove low molecules and lipids, and the dried residue was further extracted with boiling distilled water (dH_2O, 100 ^oC, material-solvent ratio 1:40, extracted for 2 h, 3×). The water extracts were combined, concentrated, and precipitated with 4-fold volume of ethanol at 4°C overnight. The

precipitate was further redissolved, dialyzed against dH_2O with cut-off 3500 Da, and lyophilized, yielding the crude polysaccharide fraction (SMAP) from the aerial parts of *S. miltiorrhiza*.

SMAP (380 mg) was dissolved in dH_2O (20 mL), filtered (0.45μm), and then applied to an anion-exchange chromatography column packed with DEAE-Sepharose Fast Flow (4.6 × 60 cm, Beijing Rui Da Heng Hui Science Technology Development Co. Ltd.). The neutral fraction was initially obtained from the eluate of 1500 mL dH_2O (1 mL/min), and an acidic fraction (SMAP-A) was further obtained from the eluates of 0-1.5 mol/L NaCl solution (2 mL/min) followed by dialysis and freeze-drying. The elution profile of the acidic fraction was monitored using the phenol-sulfuric acid assay (Dubois, Gilles, Hamilton, Rebers, & Smith, 1956).

SMAP-A (20 mg/in 5 mL in dH_2O) was applied to a size exclusion chromatography column packed with Sepharose 6FF matrix (2.5 cm× 100 cm, Beijing Rui Da Heng Hui Science Technology Development Co. Ltd) and eluted with dH_2O at 0.5 mL/min (5 mL/tube). The purified fraction was pooled after monitoring using the phenol-sulfuric acid assay, and one homogenous fraction, SMAP-1, was obtained and used for further structural characterization and bioassays.

2.3 Structural characterization of SMAP-1

The weight-average molecular weight (*Mw*), number-average molecular weight (*Mn*), and their distribution equivalents of SMAP-1 were determined by a high-performance gel permeation chromatography (GPC) using Waters Ultrahydrogel Linear gel column (300 × 7.8 mm, at 40 ℃) connected with Waters 2410 refractive index detector. The mobile phase was 0.2 mol/L $NaNO_3$ solution, pH = 6.0, eluted at a flow rate of 0.6 mL/min. Dextran standards with known molecular weights (2.5 to 5348 kDa, all from Sigma-Aldrich except for 5348 kDa from Amresco Inc., OH, USA) were used for establishing a calibration. After dissolving by the mobile phase, the dextran standards

and SMAP-1 were injected (20 μL, 5 mg/mL), and the corresponding chromatograms were recorded.

The monosaccharide composition of SMAP-1 was quantified by capillary gas chromatography (GC) after methanolysis and trimethylsilyl (TMS)-derivatization, as described previously (Chambers & Clamp, 1971; Nyman, Aachmann, Rise, Ballance, & Samuelsen, 2016). Briefly, 1 mg of SMAP-1 was hydrolyzed by anhydrous 3 mol/L HCl in methanol at 80 ℃ for 20 h. 100 μg mannitol was used as an internal standard. The volatile monosaccharides were obtained by derivatization with hexamethyldisilazane (HDMS) and trimethylchlorosilane (TMCS) and were further analyzed using a Trace^{TM} 1300 GC (Thermo Scientific^{TM}). The relative amount of each monosaccharide was processed and calculated using a Chromelion Software v.6.80 (Dionex Corporation, Sunnyvale, CA, USA) based on retention time and peak integration compared to TMS-derived standards, including arabinose (Ara), rhamnose (Rha), fucose (Fuc), xylose (Xyl), mannose (Man), galactose (Gal), glucose (Glc), glucuronic acid (GlcA) and galacturonic acid (GalA).

The contents of phenolic compounds and protein in SMAP-1 were quantitatively determined using the Folin-Ciocalteu assay (Singleton & Rossi, 1965) and the Bradford protein assay (Bradford, 1976), respectively.

The glycosidic linkage pattern of SMAP-1 was analyzed by GC-MS after per-methylation based on the monosaccharide composition determined above, as previously described (Ciucanu & Kerek, 1984; Pettolino, Walsh, Fincher, & Bacic, 2012; Wold et al., 2018). Briefly, 2 mg of SMAP-1 was processed with carboxyl reduction using sodium borodeuteride ($NaBD_4$) after being activated by carbodiimide to reduce the uronic acids (GalA and GlcA) to their corresponding neutral sugars (Kim & Carpita, 1992). The polymer was then methylated by methyl iodide under NaOH in dimethyl sulfoxide and further hydrolyzed with 2.5 mol/L trifluoroacetic acid, followed by

reduction with $NaBD_4$ and acetylation. The partially methylated alditol acetates (PMAA) were extracted with dichloromethane and analyzed qualitatively and quantitatively on a GCMS-QP2010 (Shimadzu, Kyoto, Japan) based on the different retention times and characteristic mass spectra. Details of regents and GC-MS conditions can be found in our previous publication (Wold et al., 2018). The analysis of linkage patterns and amounts was related to the molar percent of monosaccharides and the effective carbon-response factors were used to quantify PMAA fragments (Sweet, Shapiro, & Albersheim, 1975; Zou et al., 2017).

The functional groups present in SMAP-1 were analyzed by Fourier-transformed infrared spectroscopy (FT-IR). 10 mg of SMAP-1 and 200 mg of potassium bromide (KBr) were ground and dried under the baking lamp, and then pressed into a 1 mm pellet. KBr was used as a blank for infrared scanning in the range 4000 cm^{-1} to 500 cm^{-1} (Perkin Elmer, Waltham, MA, USA).

A Bruker Advance III HD 800 MHz NMR spectrometer (Bruker, Fällanden, Switzerland) equipped with a 5-mm cryogen probe CP-TCI z-gradient probe (Bruker, Rheinstetten, Germany) was used to acquire signals for ^{1}H (with continuous-wave pre-saturation, pulse program "zgpr"), ^{13}C (pulse program "zrestse.dp.jcm800"), ^{1}H-^{13}C heteronuclear multiple-bond correlation spectroscopy (HMBC, pulse program "awhmbcgplpndqfpr" and "awshmbcctetgpl2nd.m"), ^{1}H-^{13}C heteronuclear single quantum coherence spectroscopy (HSQC, pulse program "awhsqcedetgpsisp2.3-135pr" and "awshsqc135pr"), ^{1}H-^{1}H correlation spectroscopy (COSY, pulse program "cosygpprqf"), ^{1}H-^{1}H rotating-frame nuclear overhauser effect spectroscopy (ROESY, pulse program "roesyph") and ^{1}H-^{1}H total correlation spectroscopy (TOCSY, pulse program "dipsi2phpr") spectra of SMAP-1. The sample was exchanged and redissolved in D_2O (99.9%, Sigma), and 2,2,3,3-tetradeuterio-3 - (trimethylsilyl) - propanoic acid sodium (TMSP) was used to calibrate the chemical shift at 0 ppm. All spectra were

recorded at 60 °C and were analyzed using MestReNova software (Ver.6.0.2, Mestrelab Research S.L., Spain).

2.4 Effects of SMAP-1 on experimental colitis in mice

2.4.1 Animal experimental design

Animal experiments were conducted under the supervision of the Ethics Committee for Animal Experiment at Sichuan Agricultural University (Confirmation number: DYXY141642008). Thirty male C57BL/6N mice (6 weeks old) were purchased from Beijing Vital River Laboratory Animal Technology Co., Ltd (Beijing, China) and maintained for one week to adapt to the new environment (24 ± 1 ℃). In the current study, DSS was used to induce experimental UC, which has been reported to have many similarities to human UC symptoms (Chassaing, Aitken, Malleshappa, & Vijay-Kumar, 2014).

Mice were divided into five experimental groups: (a) normal control (NC) group (regular drinking water + saline, n = 6), (b) colitis control (DSS group) (3% DSS + saline, n = 6), (c)- (e) different dosages of SMAP-1 groups (3% DSS + SMAP-1, n = 6). Firstly, mice in groups (c)-(e) were pretreated with three doses of SAMP-1 (50 mg/kg, 100 mg/kg, 150 mg/kg, 0.1 mL/10 g) for 7 days by oral gavage (the 1^{st} to 7^{th} day) before DSS was administrated in drinking water, while mice in groups (a) and (b) were orally administrated with an equal volume of saline. After 7 days of pretreatment, 3% DSS was given through drinking water to groups (b)-(e) for 7 days (the 8^{th} to 14^{th} day), while group (a) was given regular drinking water, as normal control. Saline and different dosages of SMAP-1 were simultaneously given to the corresponding groups by gavage. Body weight, diarrhea, and bloody stool were observed and measured daily for evaluating the disease activity index (DAI) according to the DAI scoring rules (Jia et al., 2015) (**Table S1**). On the 15^{th} day, mice were euthanized with carbon dioxide

followed by cervical dislocation, and blood, cecal contents, and colonic tissues were collected. The length of the colon was measured, and colonic tissues, serum, and cecal content were stored at -80 ℃ for further studies.

2.4.2 Histological analysis and determination of inflammatory and oxidative stress indexes in the colon

The distal colon was embedded in paraffin and sliced (5 μm), and then the sections were stained with hematoxylin and eosin (H&E, Hematoxylin-Eosin Staining Kit, Beijing Solarbio Science and Technology co., Ltd. Beijing, China). Sections were photographed with Nikon eclipse 80i microscope (Nikon Instruments, Melville, NY, USA) at 100 and 200 × magnification. Histological evaluation index (HAI) was determined using the evaluation criteria listed in **Table S2.**

The proximal colon was homogenized and resuspended with PBS, and the supernatant was collected after centrifuging for the determination of the contents of myeloperoxidase (MPO), IL-1β, IL-6, IL-10, TNF-α, and TGF-β using ELISA kits (Shanghai Enzyme-linked Biotechnology Co., Ltd., Ruixin Biotechnology Co., Ltd, China). The levels of superoxide dismutase (SOD), malondialdehyde (MDA), and glutathione peroxidase (GSH-PX) in colonic tissues were measured using biochemical assay kits (Nanjing Jiancheng Bioengineering Institute, Nanjing, China) according to the manufacturer's instructions.

2.4.3 Determination of LPS and oxidative indicators in serum

The content of lipopolysaccharide (LPS) in serum was determined using an ELISA kit, and the contents of SOD, MDA, and GSH-PX in serum were determined using biochemical assay kits according to the manufacturer's instructions.

2.4.4 Real-time quantitative PCR (RT-qPCR)

The total RNA of proximal colon tissue was extracted with Trizol reagent (Biomed, RA101-02, China) according to the manufacturer's instructions. The isolated total RNA

(5 μg/μL) was reversely transcribed into cDNA using the M-MLV4 First-Strand cDNA Synthesis Kit (Takara Biotechnology, Co., Ltd, Dalian, China) after measuring the RNA concentration with a microspectrophotometer (Thermo Scientific, NanoDrop™ One/OneC, USA). Real-time PCR was performed using the SYBR premix Ex Taq. II Kit (Takara biotechnology, Co., Ltd., Dalian, China). β-actin was used as an internal parameter to determine the relative expressions of target genes calculated by the $^{\triangle\triangle}$Ct method. All primer sequences for RT-qPCR are listed in **Table S3.**

2.4.5 Untargeted metabolomic analysis

Serum preparation and untargeted metabolomic analysis were carried out by Novogene Co., Ltd. (Beijing, China). Briefly, serum (100 μL) was resuspended with 400 μL of pre-chilled 80% methanol and 0.1% formic acid (FA) using the vortex. Then, samples were incubated on ice for 5 min and centrifuged at 15 000 *g*, 4°C for 20 min. The supernatant was diluted to a final concentration containing 53% methanol with LC-MS grade water. The supernatant after further centrifuge at 15 000 *g*, 4°C for 20 min was injected into a LC-MS/MS with a Vanquish UHPLC system (Thermo Fisher, Germany) coupled with an Orbitrap Q ExactiveTMHF-X mass spectrometer (Thermo Fisher, Germany) for analysis. Raw data from UHPLC-MS/MS were processed using the Compound Discoverer 3.1 (CD3.1, Thermo Fisher), including peak alignment, peak picking, and quantification for each metabolite. Metabolites were further annotated using the Kyoto Encyclopedia of Genes and Genomes (KEGG) database (https://www.genome.jp/kegg/pathway.html), HMDB database (https://hmdb.ca/metabolites) and Lipid Maps database (http://www.lipidmaps.org/). Graphical representations of PCA and PLS-DA were generated using metaX software. The univariate analysis (t-test) was applied to calculate the statistical significance (P-value). The metabolites with VIP > 1 and *p*-value < 0.05 and FC ≥ 2 or FC ≤ 0.5 were considered to be differential metabolites. The functions of these metabolites and

metabolic pathways were analyzed using the MetaboAnalyst 5.0 (https://www.metaboanalyst.ca/).

2.5 Anti-inflammatory and anti-oxidative effects *in vitro*

2.5.1 Cell culture

Intestinal porcine enterocyte cells (IPEC-J2) were cultured in Dulbecco's modified Eagle's medium (DMEM, Gibco, Waltham, MA, USA) supplemented with 10% fetal bovine serum (FBS; Gibco; Waltham, MA, USA) and 1% penicillin–streptomycin (Gibco, Waltham, MA, USA). They were cultured in an incubator at 37 ℃ with 5% CO_2.

2.5.2 Experimental design

IPEC-J2 cells were seeded in 6-well plates and cultured for 24 h (2×10^5 cells/well). Different final concentrations of SMAP-1 (5, 10, 20 μg/mL) or 5-methoxyindole-3-carboxaldehyde (5-MC, 5, 10, 20 μg/mL) were administrated and cultured with cells for 12 h, followed by another 12 h of incubation with 20 μg/mL of LPS to induce inflammation on cells, as earlier described (Zou et al., 2022). After co-cultivation, supernatants were collected to determine the protein contents of CAT, GSH-PX, and SOD by ELISA kits, as described in section 2.4.2. Cells were collected using Trizol reagent to extract total RNA, and RT-qPCR was further performed to determine the gene transcription levels of CAT, GSH-PX, and SOD, and the levels of proteins associated with Nrf2/Keap1 signaling pathways, as described in section 2.4.4. Primers used for RT-qPCR are listed in **Table S3**. Cytotoxicity of LPS, SMAP-1, and 5-MC on IPEC-J2 cells was tested on 96-well plates according to previous experimental methods (Zou et al., 2022).

2.6 Statistical analysis

All data except for metabolomic analysis were expressed as the mean± S.D. and analyzed and plotted in GraphPad Prism 8.0 (California, USA). Statistical analysis was performed using a one-way ANOVA analysis of variance and LSD test in SPSS 22.0 (IBM Corp., Armonk, New York, USA).

3 Results and Discussion

3.1 Extraction and isolation of SMAP-1

A crude polysaccharide fraction, SMAP, was obtained from the water extract of the aerial parts of *S. miltiorrhiza* (~15%, w/w). A small amount of neutral polysaccharide fraction (8.6% mass of SMAP) and a larger amount of acidic polysaccharide fraction (SMAP-A, 91.4% mass of SMAP) were obtained after anion-exchange chromatography (**Fig. 1A**). A homogeneous fraction, SMAP-1, was further obtained from SMAP-A by size exclusion chromatography (**Fig. 1B**).

3.2 Structural characterization of SMAP-1

3.2.1 Determination of chemical compositions, molecular weights, and glycosidic linkage pattern

After methanolysis, TMS-derivatization, and GC analysis, SMAP-1 was found to be composed mainly of GalA, followed by Ara, Gal, Rha, and Glc (**Fig. 1C**), with a molar ratio of 19.7:1.4:1.4:1.3:1. Trace amounts of GlcA, Xyl, Man, and Fuc were present in SMAP-1. A small amount of protein (1.4%) and a trace amount of phenolics (0.4%) were detected in SMAP-1. The *Mw, Mn,* and polydispersity of SMAP-1 were 26.3 kDa, 5.52 kDa, and 4.77, respectively, as determined by GPC, and a single symmetric peak was observed during the elution (**Fig. S1A)**.

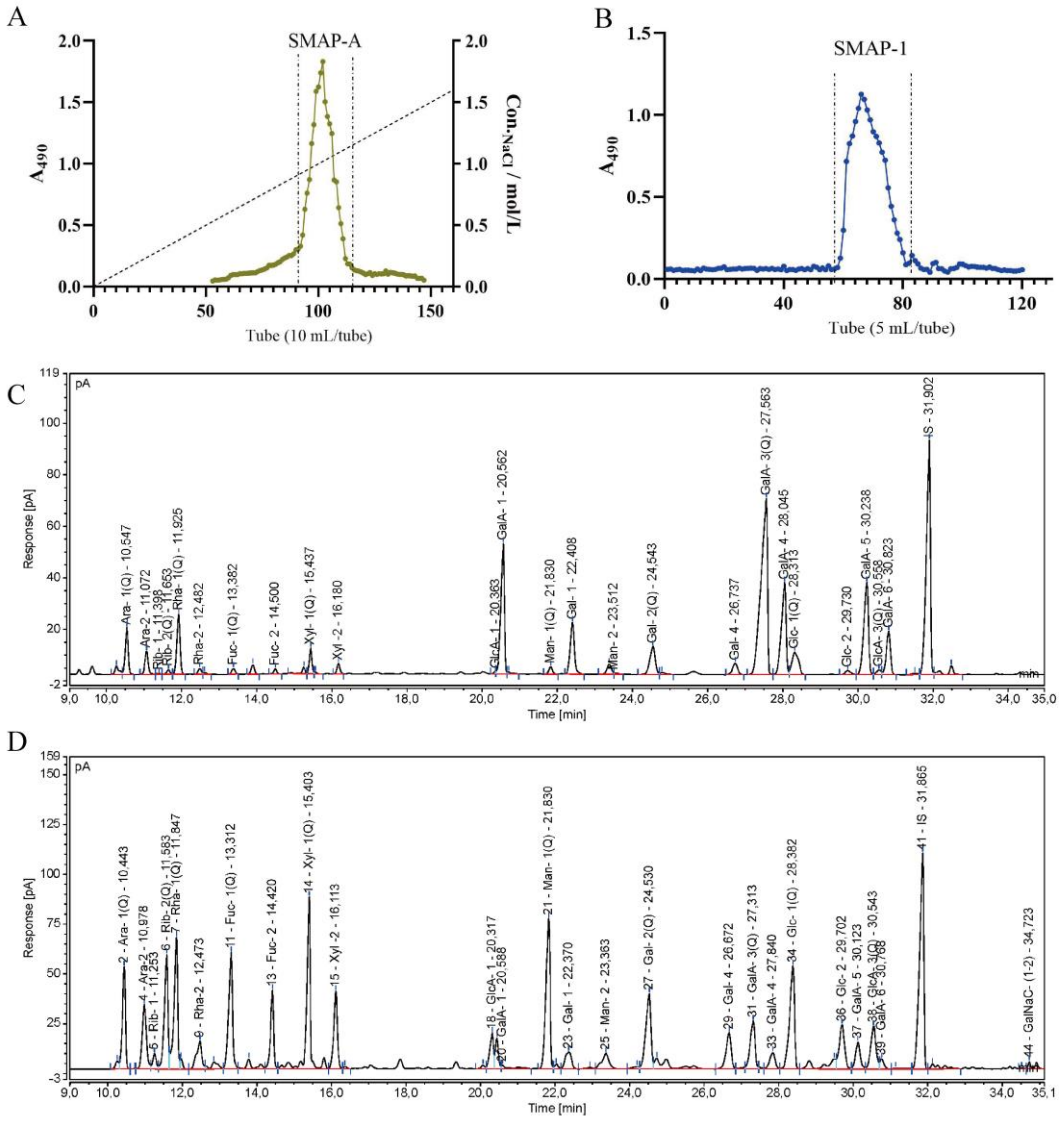

Fig. 1. Elution profiles of anion-exchange chromatography (A) and size exclusion chromatography (B) and monosaccharide composition (C) of SMAP-1. Each monosaccharide derivative was present in the forms of different isomers, resulting in different peaks in the GC chromatogram, and the peaks marked with (Q) were used for quantification analysis based on integration of peaks of TMS-derivatized standards (D).

The glycosidic linkage pattern of SMAP-1 is shown in **Table 1**, presented as relative amount in mol% of each monosaccharide determined after methanolysis and TMS-derivatization. The GC chromatogram and mass spectra of the major peaks in the

GC chromatogram are shown in **Fig. S2**. A large amount of 1,4-linked α-Gal*p*A (68.9 mol%) and smaller amounts of different linkage types of Gal*p*A were detected in SMAP-1, suggesting that SMAP-1 could be a typical pectic polysaccharide (Mohnen, 2008). A long homogalacturonan (HG) composed of 1,4-linked α-Gal*p*A was shown to be present in SMAP-1 due to the relatively higher content of Gal*p*A compared with Rha*p*. This linear homopolymer of 1,4-α-homogalacturonan can be dispersed with 1,2-linked Rha*p* units, including 1,2-linked and 1,2,4-linked α-L-Rha*p* **(Table 1)**, which confirmed that there could be a rhamnogalacturonan I region (RG-I) present in SMAP-1 in addition to the long HG linear chain (Kaczmarska, Pieczywek, Cybulska, & Zdunek, 2022; Mohnen, 2008; Zaitseva, Khudyakov, Sergushkina, Solomina, & Polezhaeva, 2020). Arabinan, galactan, and/or arabinogalactan are usually attached to the RG-I at *O*-4 of the rhamnosyl unit and form the side chains of the RG-I backbone (S.-S. Li et al., 2018). These side chains typically consist of 1,5-α-Ara*f* (arabinan), 1,4-α-Gal*p* (type I arabinogalactan, AG-I), 1,3,6-α-Gal*p*, and terminal (T)-Ara*f* (type II arabinogalactan, AG-II) (Pettolino et al., 2012). The low amount of terminal and 1,5-linked α-Ara*f* fragments in SMAP-1 indicated the presence of arabinans (Kaczmarska et al., 2022). And the small amount of 1,4- and 1,3,6-linked β-Gal*p* showed that SMAP-1 could consist of both AG-I and AG-II side chains (Kaczmarska et al., 2022). Trace amounts of T-Xyl*p* and T-Rha*p* were also observed.

The results of monosaccharide composition and glycosidic linkage patterns indicated that SMAP-1 could be a typical pectic polysaccharide. This is the first report on the isolation of pectin from the aerial parts of *S. miltiorrhiza*, in addition to a disaccharide consisting of fructose and Glc detected in 80% ethanol extracts (Zeng et al., 2017). A neutral fraction composed mainly of Glc and Gal (Jiang et al., 2020), and a hemicellulose-based polysaccharide composed of the 4-β-$_D$-Xyl*p* backbone (Zhao et al., 2020) were previously identified from the roots of *S. miltiorrhiza.* And recently, a

possible pectic polysaccharide was isolated from these roots, but no NMR elucidation was performed (Jing et al., 2022).

Table 1. The linkages pattern (mol%) of SMAP-1 determined by GC–MS after methylation

Type of linkage		Rt/min	Primary fragments	mol %
GalA	T-Gal*p*A	17.17	47,118,162,207	2.2
	1,4-Gal*p*A	19.88	47,118, 162, 235	68.9
	1,3,4-Gal*p*A	20.72	47, 118, 307	2.6
	1,2,4-Gal*p*A	21.19	47, 190, 235	0.4
Ara	T-Ara*f*	12.42	45,118,161,162	3.5
	1,5-Ara*f*	15.56	118, 162, 189	2.0
	1,3,5-Ara*f*	17.55	118, 261	1.2
Gal	T-Gal*p*	17.17	45, 118, 162, 205	0.9
	1,4-Gal*p*	19.88	45, 118, 162, 233	1.5
	1,3,6-Gal*p*	22.63	118,189,234,305	1.0
	1,6-Gal*p*	20.42	118,162,189,233	0.8
	1,3-Gal*p*	19.43	118,161,234,277	0.5
Glc	1,4-Glc*p*	19.20	45,118,162,233	4.0
Rha	T-Rha*p*	13.31	118,131,162,175	0.8
	1,2-Rha*p*	15.56	131,190	2.6
	1,3-Rha*p*	15.93	118,131,234	0.8
	1,2,4-Rha*p*	17.90	190, 203	1.5
Xyl	T-Xyl*p*	13.31	118,131, 162	2.1

3.2.2 FT-IR analysis

The FT-IR was used to characterize the functional groups in SMAP-1 after scanning in a range of 4000 cm^{-1}-500 cm^{-1}. As shown in **Fig. S1B**, a strong peak at 3382 cm^{-1} and a lower one at 2935 cm^{-1} belonging to the stretching vibrations of O-H and C-H groups (including CH, CH_2, and/or CH_3), respectively (Li et al., 2020), were observed.

The strong absorption peak at 1740 cm^{-1} and 1606 cm^{-1} are stretching vibrations of methyl esterified and non-esterified carboxyl groups, respectively (Chylińska, Szymańska-Chargot, & Zdunek, 2016; Kyomugasho, Christiaens, Shpigelman, Van-Loey, & Hendrickx, 2015), indicating the presence of esterified GalA units in SMAP-1. The bands at 1417 cm^{-1} and 1236 cm^{-1} were characterized as the bending vibrations of CH_2 and CH_3CO stretching, respectively. And in the region of 1200-900 cm^{-1}, intense bands at 1100 and 1019 cm^{-1} were attributed to glycosidic bonds (C-O) and pyranoid rings (C-C), respectively (Kpodo et al., 2017).

3.2.3 NMR elucidation

The structure of SMAP-1 was further characterized by NMR, including 1D NMR spectra of ^{1}H and ^{13}C NMR (**Fig. S1C** and **Fig. S1D**) and 2D NMR spectra, including HSQC **(Fig. 2A)**, HMBC **(Fig. 2B)**, COSY (**Fig. S1E**) and TOCSY (**Fig. S1F**). Through-space ^{1}H-^{1}H correlations of SMAP-1 were measured by ROESY, which are presented in **Fig. 2C**. Residues were assigned based on the glycosidic linkages observed in section **3.2.1** (**Table 1**) and compared with the reported chemical shift values in the literature, as described below. Chemical shift values of residues in SMAP-1 are presented in **Table 2,** and important correlations in HMBC, TOCSY, and ROESY spectra that were used to assign protons/carbons of inter- and/or intra-residues were listed in **Table 3**. Specific correlations in HMBC and ROESY spectra, as shown in **Fig. 2E**, are used to characterize the sequences of GalA residues in SMAP-1. However, signals of some residues or certain atoms could not be recorded due to their low amounts of existence in SMAP-1, and their correlations with the adjacent sugar residue were mostly undetectable.

→4)-α-Gal*p*A-6-*O*-Me-(1→ (residue A, A'). According to the results of FT-IR and the presence of a cross peak at $\delta_{H/C}$ 3.82/55.1 ppm in the HSQC spectrum (**Fig. 2A**, cross-peak ***O*-Me**), methyl (-OCH_3) esterified GalA units are present in SMAP-1, which could be located at C-6 (carboxyl group) of 1,4-linked GalA in the HG region (Mohnen,

2008; Yao, Wang, Yin, Nie, & Xie, 2021; Zaitseva et al., 2020). The anomeric signals at $\delta_{H/C}$ 4.91/102.6 and 4.97/102.7 ppm, and the weaker one at $\delta_{H/C}$ 5.17/102.1 ppm in the HSQC spectrum (**Fig. 2A**, cross-peak **A1, A'1**) were assigned to the H-1/C-1 of residue →4)-α-Gal*p*A-6-*O*-Me-(1→ under different spin systems according to the assignments in the literature (Kostálová, Hromádková, & Ebringerová, 2013; Shakhmatov, Atukmaev, & Makarova, 2016). The assignment of H-2/C-2 to H-5/C-5 of residue **A** and **A'** was performed separately according to the correlations between H-1 (4.91/4.97 ppm) and C-2, C-3, C-4, and/or C-5 in the HMBC spectrum (**Fig. 2B**, cross-peak **A/A'-H1/C2**, **A/A'-H1/C3**, etc.), the correlations between H-1 and H-2 in COSY spectrum (**Fig. S1E,** cross-peak **A/A'-H1/H2**), and the correlations between protons in the same sugar ring (H-1 to H-5) in TOCSY spectrum (**Fig. S1F,** cross-peak **A/A'-H1/H2**, **A/A'-H1/H3**, etc.), as summarized in **Table 3**. Importantly, the down-yield shifts of H-5 at 5.11 and 5.06 ppm (cross-peak **A5, A'5** in HSQC spectrum) and the high-yield shift of C-6 from 177.9 to 173.6 ppm (**Fig. 2B**, cross-peak **A/A'-H5/C6** at $\delta_{H/C}$ 3.82/173.6 ppm in HMBC spectrum) were representative signals that can be observed due to methyl-esterification at C-6 of Gal*p*A. The correlation of C-6 with the proton of the *O*-Me group (3.82 ppm) in the HMBC spectrum (**Fig. 2B**, cross-peak ***O*-Me-H/A/A'-C6**) verified the location of methyl-esterification, which is consistent with the results of earlier reports (Kostálová et al., 2013; Rosenbohm, Lundt, Christensen, & Young, 2003). The down-yield shifts of H-4/C-4 demonstrated *O*-glycosylation at C-4 of Gal*p*A, which accounted for more than 60 mol% in SMAP-1 (**Table 1**). However, regarding the spin system related to anomeric atoms at $\delta_{H/C}$ 5.17/102.1 ppm, fewer carbon signals were found in the HMBC spectrum possibly due to the relatively low amount, but the weak cross peak at 5.17/173.6 ppm (**Fig. 2B**, cross-peak **A-H5/C6**) manifested that it should be a methyl-esterified residue. The sequence of residues **A** and **A'** in SMAP-1 was assigned followed by the description of residues **B** and **B'**.

→4)-α-Gal*p*A-(1→ (residue B, B'). Being similar to the way of the assignment for residue **A** and **A'**, the presence of →4)-α-Gal*p*A-(1→ with no methyl-esterification was verified due to the regular shift values of the carboxyl group at C-6 at 177.9 ppm, as shown in the inserted selective HMBC plot in **Fig. 2B** (cross-peak **B-$_{H5/C6}$** and **B-$_{H4/C6}$**), where a distinct shift value at 177.9 ppm was observed, being different from that of methylated carboxyl group at 173.6, and the one from the acetyl group at 176.5 ppm (***O*-Ac**). Regular chemical shift values at 4.67 and 4.70 ppm were also observed and assigned to H-5 of residue **B** and **B'** respectively due to their correlation with C-6 at 177.9 ppm (cross-peak **B-$_{H5/C6}$** and **B'-$_{H5/C6}$** in **Fig. 2B**), similar to the shift values reported in previous studies (Dénou et al., 2022; Kostálová et al., 2013; Shakhmatov et al., 2016). And accordingly, the assignment of H-1/C-1 to H-1/C-4 was performed based on the correlations in the HMBC and TOCSY spectra, as shown in **Table 3, Fig. 2B** and **Fig. S1F**, and shift values in the literature (Huang et al., 2021; Shakhmatov, Belyy, & Makarova, 2018; Zou et al., 2014).

At the same time, residues **A, A', B,** and **B'** are the main units composed in SMAP-1 due to the high amounts of 1,4-linked Gal*p*A determined in GC-MS and high absorption peaks of the esterified and non-esterified uronic acid observed in FT-IR. Signals of important correlations between H-1/H-5/C-1 of residue **A** and C-4/H-4 of residue **B**', correlations between H-1/H-5 of residue **A'** and H-4 of residue **A**, and connection between H-5/C-1 of residue **B'** and H-4/H-5 of residue **B**, indicated the presence of the linkage pattern: residue **A** → residue **B'**, residue **A'** → residue **A**, and residue **B'** → residue **B,** respectively, as shown in sequence 1 in **Fig. 2E** and summarized in **Table 3**. Moreover, the correlations between C-1/H-1 of residue **B'** and H-5/C-5/H-4/C-4 of residue **A** and the correlations between C-1 of residue **B** and H-5 of residue **B'** indicated the presence of the linkage pattern: residue **B'** → residue **A** and residue **B** → residue **B'**, as shown in sequence 2 in **Fig. 2E** and **Table 3**. Therefore, the

sequence of these residues could be mainly composed of **A'-A-B'-B** and **B-B'-A-A'**, as shown in **Fig. 2E**.

→4)-α-Gal*p*A-3-*O*-Ac-(1→ (residue C). A cross peak ***O*-Ac** at $\delta_{H/C}$ 2.09/23.2 ppm and $\delta_{H/C}$ 2.18/23.5 ppm in the HSQC spectrum (**Fig. 2A**) indicated the presence of acetyl group (CH_3CO-) in SMAP-1 (Yao et al., 2021). The location of the *O*-acetyl groups in residue **C** could not be assigned from the HMBC spectrum, as only one correlation between its proton and the carbonyl group could be observed (***O*-Ac** in **Fig.2B**). However, the down-yield shift of H-3 at 5.18 ppm was observed, which suggested the site of acetyl group at *O*-3. Other signals of C-2/H-2 to C-5/H-5 were assigned according to their correlations with H-3 in COSY (cross-peak **C-H2/H3** in **Fig. S1E**), HMBC (cross-peak **C-H3/C4** in **Fig. 2B**), TOCSY, and ROESY (**C-H3/H4** in **Fig. 2C**) spectra, and the correlations between C-6 and H-4/5 in HMBC spectrum (cross-peak **C-H4/C6** and **C-H5/C6** in **Fig. 2B**), as shown in **Table 3**, as well as based on the shift values reported in the literature (Huang et al., 2021; Komalavilas & Mort, 1989; Patova et al., 2019; Zhao et al., 2017a).

→4)-α-Gal*p*A (residue D) and →4)-β-Gal*p*A (residue F). The cross peak at $\delta_{H/C}$ 5.31/95.0 (**D1** in **Fig. 2A**) and $\delta_{H/C}$ 4.59/99.0 ppm (**F1** in **Fig. 2A**) correspond to α and β formations of reducing end Gal*p*A in pectin, respectively, as described in previous studies (Shakhmatov et al., 2016; Shakhmatov et al., 2018; Zou et al., 2021). Being similar to the assignment introduced in aforementioned residues, the rest of the atoms of H-2/C-2 to H-5/C-5 were assigned based on their correlations with H/C-1 and correlations between all atoms in COSY, TOCSY, HMBC, and ROESY spectra, as shown in **Fig. S1E, Fig. S1F, Fig. 2B,** and **Fig. 2C** respectively. Detailed correlations in HMBC, TOCSY, and ROESY of signals from residues **D** and **F** are summarized in **Table 3.**

α-Ara*f*-(1→, →5)-α-Ara*f*-(1→ and →3,5)-α-Ara*f*-(1→ (residue G, H and I). The anomeric carbon of furanose, Ara*f* in this study, is commonly observed in the range of 103 to 112 ppm (Yao et al., 2021), which indicated the cross peaks observed in the anomeric region of HSQC spectrum at $\delta_{H/C}$ 5.15/110.2, 5.21/111.1, 5.09/110.4 and 5.11/110.5 (cross-peak **G1, H1,** and **I1** in **Fig. 2A**) belong to Ara*f* residues of SMAP-1. This anomeric carbon and protons were further assigned according to the shift values reported by Shakhmatov et al. (2018). Further, cross peaks at $\delta_{H/C}$ 5.15/86.8 ppm and $\delta_{H/C}$ 5.09/85.2 ppm in the HMBC spectrum (**G-$_{H1/C4}$** and **H-$_{H1/C4}$** in **Fig. 2B**) were annotated to the inter-unit correlation of H-1 with C-4 of residue **G** and **H**, respectively. In addition, the cross peak at $\delta_{H/C}$ 5.11/68.7 ppm suggested the intra-unit correlation between H-1 of residue **I** and C-5 of residue **H**, where the down-yield shift of C-5 at 68.7 ppm was affected by *O*-glycosylation. While, the regular shift values of C-5 at 64.4 or 64.5 ppm, shown as negative cross peaks at $\delta_{H/C}$ 3.73/64.4 and 3.82/64.5 ppm in HSQC (**G5** in **Fig. 2A**), could be attributed to the terminal Ara*f* (residue **G**). Other protons and carbons of residues **G**, **H,** and **I** were found in the HSQC spectrum (**Fig. 2A**) according to the reported shift values in the literature (Li, Chen, Liu, Xu, & Zhang, 2021; Shakhmatov et al., 2016; Shakhmatov et al., 2018), as most intra-unit H-C or H-H correlations could not be observed because they are present only in small amounts in SMAP-1.

→2)-α-Rha*p*-(1→ and →2,4)-α-Rhap-(1→ (residue J and **K).** The presence of -CH_3 groups at $\delta_{H/C}$ 1.28/19.8, 1.30/19.9, and 1.39/19.9 ppm in HSQC (**J6, K6** in **Fig. 2A**) could be signals from H-6/C-6 of Rha*p* (Yao et al., 2021), and the weak anomeric atoms (H-1/C-1) and H-2/C-2 were observed at $\delta_{H/C}$ 5.28/100.2 ppm (**J1/K1**) and 4.11/78.2 ppm (**J/K2**) in the HSQC (**Fig. 2A)**, respectively, according to the earlier reported shift values (Shakhmatov et al., 2018). Correlations between H-6 and C-5 at $\delta_{H/C}$ 1.28/72.0 and 1.30/71.0 ppm (**J_{H6-C5}** in **Fig. 2B**) and correlations between H-6 and C-4 at $\delta_{H/C}$ 1.28/74.8 and 1.30/75.1 of residue **J** (**J_{H6-C4}** in **Fig. 2B**) were observed in

the HMBC spectrum (Shakhmatov et al., 2018). Only a weak correlation was found between H-6 and C-5 of residue **K** at $\delta_{H/C}$ 1.39/71.0 ppm in HMBC (**$K_{H6\text{-}C5}$** in **Fig. 2B**) due to its low amount of presence in SMAP-1 (1.5 mol%), the same for its weak H-4/C-4 signals at $\delta_{H/C}$ 3.74/82.4 ppm in HSQC (Shakhmatov et al., 2018; Shakhmatov, Makarova, & Belyy, 2019). These aforementioned shift values and those of H-2/C-2 of residue **J** and **K** were assigned in accordance with previous reports (Huang et al., 2021; Shakhmatov et al., 2018; Shakhmatov et al., 2019).

Other residues including α-Gal*p*A-(1→ (residue **E**), →4)-β-Glc*p*-(1→ (residue **L**), →4)-β-Gal*p*-(1→ (residue **M**) were assigned mainly based on the reported chemical shift values in the literature (Shakhmatov et al., 2016), in addition to the H-1/H-2 correlation of residue **L** in TOCSY spectrum (**L-$_{H1/H2}$** in **Fig. S1F**). Other correlations between different protons and carbons in these residues could not be found due to the low relative amounts of presence in SMAP-1. And the signals of the anomeric and other atoms of terminal Xyl*p* were too weak to be well assigned. In summary, the aforementioned residues compose the structure of SMAP-1 as a typical pectin, mainly consisting of a long HG linear chain, followed by shorter RG-I backbones with brunches of arabinan and possible AG-I or II side chains, as shown in the proposed structure in **Fig. 2F**.

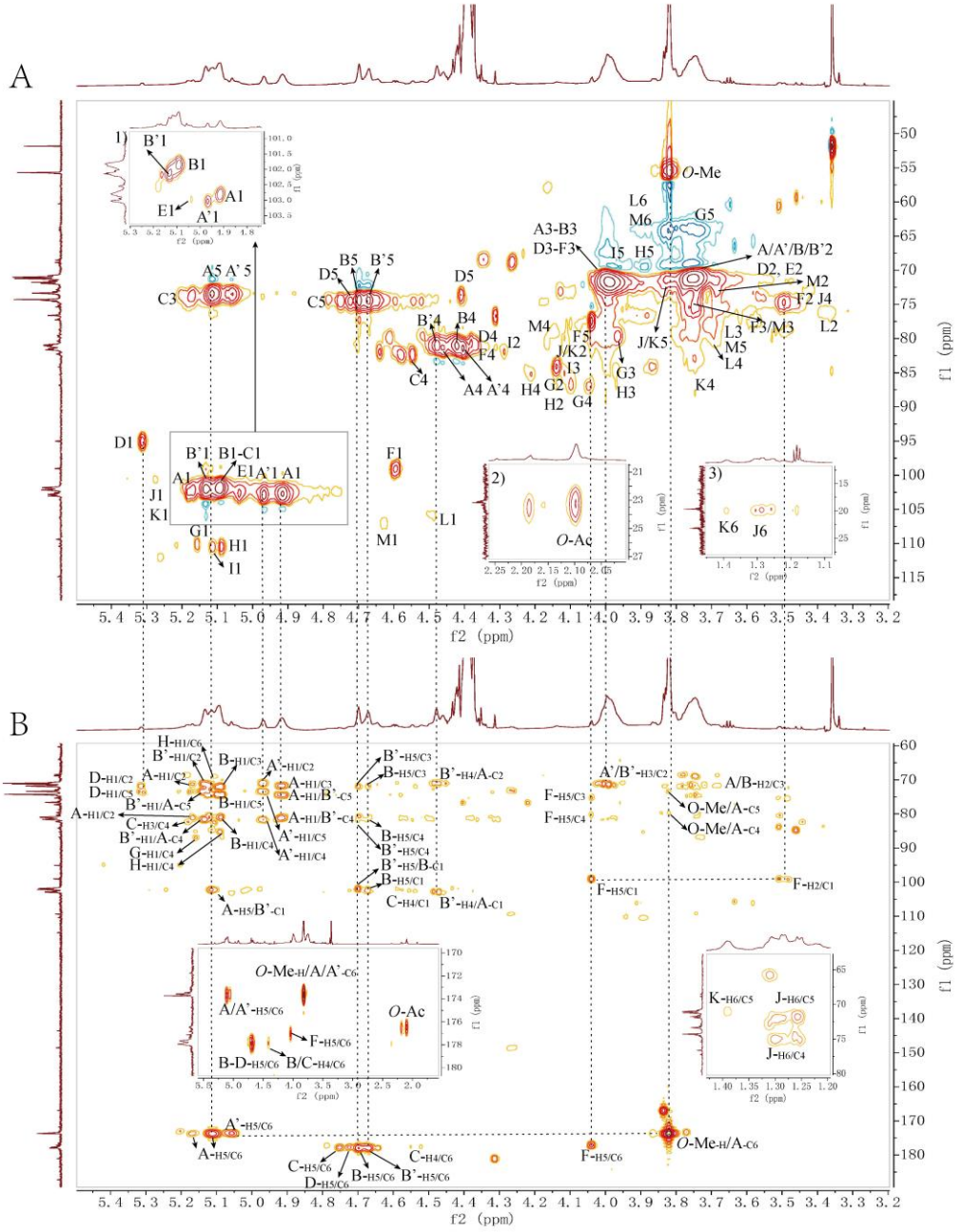

Fig. 2. NMR spectra (A-C) and the proposed structure (D-F) of SMAP-1. (A), HSQC spectrum; (B), HMBC spectrum; (C), ROESY spectrum; (D), the illustration of the sequence elucidation using ROESY and HMBC; (E), sequences of residue →4)-α-Gal*p*A-6-*O*-Me-(1→ (**A** and **A'**) and →4)-α-Gal*p*A-(1→ (**B** and **B'**) in HG region; (F), the proposed structure depicted by graphical symbols according to the symbol nomenclature for glycans (SNFG) (Varki et al., 2015).

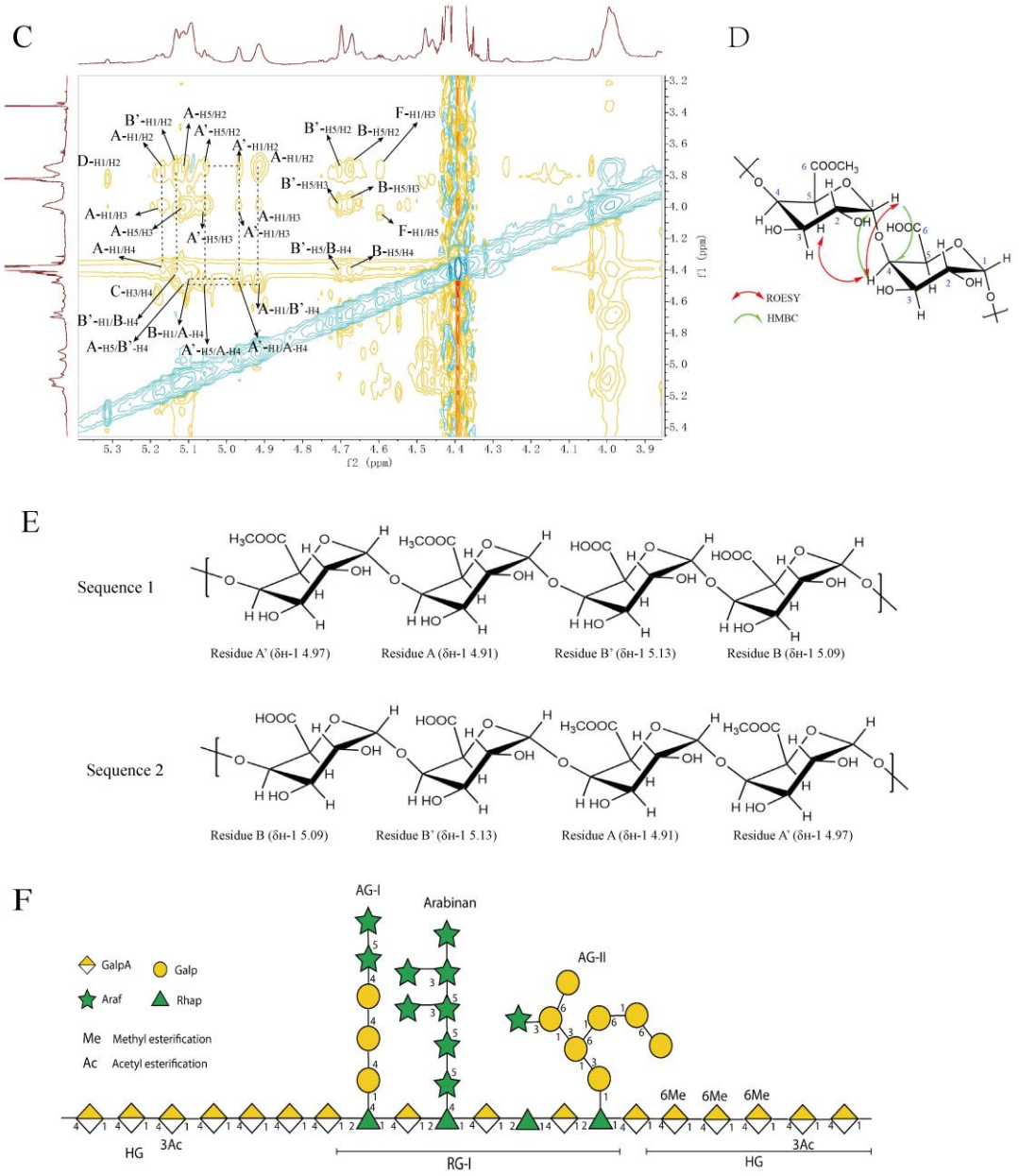

Fig.2. *(Continued)*

Table. 2 ^{1}H and ^{13}C chemical shift values (δ in ppm) of SMAP-1

Residues		H1/C1	H2/C2	H3/C3	H4/C4	H5/C5	H6/C6	OCH3
A	→4)-α-Gal*p*A-6-*O*-Me-(1→	4.91/102.6	3.75/71.6	3.97/71.6	4.46/81.6	5.11/73.4	/173.6	3.82/55.1
		5.17/102.1	3.77/71.4	3.99/n.d.	4.38/n.d.	n.d.	/173.6	
A'	→4)-α-Gal*p*A-6-*O*-Me-(1→	4.97/103.0	3.74/71.1	3.99/71.6	4.40/81.6	5.06/73.4	/173.6	3.82/55.1
B	→4)-α-Gal*p*A-(1→	5.09/101.8	3.77/71.3	3.98/71.9	4.42/80.9	4.67/74.4	/177.9	
B'	→4)-α-Gal*p*A-(1→	5.13/101.9	3.76/71.1	3.99/71.9	4.48/80.9	4.70/74.4	/177.9	
C	→4)-α-Gal*p*A-3-*O*-Ac-(1→[&]	5.09/101.8	4.01/n.d.	5.18/73.7	4.54/82.4	4.75/74.6	/177.7	
D	→4)-α-Gal*p*A	5.31/95.0	3.83/72.0	3.99/71.6	4.38/80.8	4.40/73.4	/177.7	
E	α-Gal*p*A-(1→*	5.04/102.5	3.83/72.0	3.98/71.5	4.41/73.6	4.72/74.6	/177.8	
F	→4)-β-Gal*p*A	4.59/99.0	3.49/74.7	3.76/75.6	4.40/80.1	4.04/77.5	/177.1	
G	α-Ara*f*-(1→	5.15/110.2	4.14/84.2	3.96/79.6	4.05/86.8	3.73/64.4		
		5.21/111.1				3.82/64.5		
H	→5)-α-Ara*f*-(1→	5.09/110.4	4.14/84.2	3.96/79.2	4.21/85.4	3.88/68.7		
I	→3,5)-α-Ara*f*-(1→	5.11/110.5	4.28/81.5	4.11/85.4	n.d.	3.98/68.1		
J	→2)-α-Rha*p*-(1→*	5.28/100.2	4.11/78.2	3.89/72.2	3.47/74.8	3.81/72.0	1.28/19.8	
					n.d./75.1	3.81/71.8	1.30/19.9	
K	→2,4)-α-Rha*p*-(1→	5.28/100.2	4.11/78.2	4.09/72.1	3.74/82.4	3.83/71.0	1.39/19.9	
L	→4)-β-Glc*p*-(1→*	4.48/105.7	3.36/76.8	3.70/77.0	3.68/80.0	3.62/76.1	3.89/63.9	
M	→4)-β-Gal*p*-(1→*	4.62/107.6	3.68/72.0	3.75/75.6	4.16/80.5	3.71/77.6	3.87/64.0	

Note: values of the chemical shifts were determined from the HSQC spectrum. * means low sensitivity in HSQC spectrum but it can be found when the sensitivity was set as 5; [&], *O*-Ac = *O*-$COCH_3$ with chemical shifts at δ_C 176.5 and $\delta_{H/C}$ 2.09/23.2; n.d., not detected

538 **Table 3.** Major proton and carbon correlations observed in HMBC, ROESY, and
539 TOCSY spectra of SMAP-1 (δ in ppm)

Residues	δ_H	Observed connections					
		HMBC		TOCSY		ROESY	
		δ_C	Atom (sequence)	δ_H	Atom	δ_H	Atom
→4)-α-Gal*p*A-6-*O*-Me-(1→	4.91 (**A**, H-1)	71.6	C-3 of residue **A**	3.75	H-2 of residue **A**	3.75	H-2 of residue **A**
		74.4	**C-5 of residue B' (A→B')**	3.97	H-3 of residue **A**	**4.48**	**H-4 of residue B' (A→B')**
		80.9	**C-4 of residue B' (A→B')**				
	4.97 (**A'**, H-1)	71.1	C-2 of residue **A'**	3.75	H-2 of residue **A'**	4.46	H-4 of residue **A (A'→A)**
		73.4	C-5 of residue **A'**	3.99	H-3 of residue **A'**		
		81.6	C-4 of residue **A'**				
	5.11 (**A**, H-5)	**102.1**	**C-1 of residue B' (B'→A)**	4.46	H-4 of residue **A**	3.99	H-3 of residue **A**
		173.6	C-6 of residue **A/A'**			**4.48**	**H-4 of residue B' (A→B')**
	5.06 (**A'**, H-5)	103.0	C-1 of residue **A'**			3.99	H-3 of residue **A'**
						4.46	**H-4 of residue A (A'→A)**
	5.17 (**A**, H-1)	71.4	C-2 of residue **A**			3.77	H-2 of residue **A**
		80.9	**C-4 of residue B' (A→B')**			3.99	H-2 of residue **A**
		173.6	C-6 of residue **A**			4.38	H-4 of residue **A**
→4)-α-Gal*p*A-(1→	5.09 (**B**, H-1)	71.9	C-3 of residue **B**	3.77	H-2 of residue **B**	3.99	H-3 of residue **B**
		74.4	C-5 of residue **B**	3.99	H-3 of residue **B**	**4.42**	**H-4 of residue B**
		80.9	C-4 of residue **B**				
	5.13 (**B'**, H-1)	71.1	C-2 of residue **B'**	3.76	H-2 of residue **B'**	3.76	H-2 of residue **B'**
		73.4	**C-5 of residue A (B'→A)**	3.99	H-3 of residue **B'**	**4.46**	**H-4 of residue A (B'→A)**
		81.6	**C-4 of residue A (B'→A)**	4.48	H-4 of residue **B'**		

540

541 **Table 3. (*Continued*)**

Residues	δ_H	Observed connections					
		HMBC		TOCSY		ROESY	
		δ_C	Atom (sequence)	δ_H	Atom	δ_H	Atom
→4)-α-Gal*p*A-(1→	4.48 (**B'**, H-4)	71.1	C-2 of residue **B'**	3.76	H-2 of residue **B'**	**4.91**	**H-1 of residue A (A→B')**
		102.6	**C-1 of residue A (A→B')**	3.99	H-3 of residue **B'**	5.13	H-1 of residue **B'**
	4.70 (**B'**, H-5)	71.9	C-3 of residue **B**'			3.76	H-2 of residue **B'**
		80.9	C-4 of residue **B**'			3.99	H-3 of residue **B'**
		101.8	**C-1 of residue B (B→B')**			**4.42**	**H-4 of residue B (B'→B)**
		177.9	C- 6 of residue **B**'				
	4.67 (**B**, H-5)	71.9	C-3 of residue **B**			3.77	H-2 of residue **B**
		80.9	C-4 of residue **B**			3.98	H-3 of residue **B**
		102.1	**C-1 of residue B' (B'→B)**			4.42	H-4 of residue **B**
		177.9	C- 6 of residue **B**				
→4)-α-Gal*p*A-3-*O*-Ac-(1→	5.18 (**C**, H-3)	71.1	C-2 of residue **C**	4.01	H-2 of residue **C**	4.54	H-4 of residue **C**
		80.9	C-4 of residue **C**				
	4.75 (**C**, H-5)	177.7	C-6 of residue **C**				
	4.54 (**C**, H-4)	177.7	C-6 of residue **C**				
→4)-α-Gal*p*A	5.31 (**D**, H-1)	71.6	C-3 of residue **D**	3.99	H-3 of residue **D**	3.81	H-2 of residue **D**
		73.4	C-5 of residue **D**				
→4)-β-Gal*p*A	4.59 (**F**, H-1)			3.76	H-3 of residue **F**	3.76	H-3 of residue **F**
				3.50	H-2 of residue **F**	4.04	H-5 of residue **F**
	4.04 (**F**, H-5)	80.1	C-4 of residue **F**				
		99.0	C-1 of residue **F**				
		177.1	C-6 of residue **F**				
	3.49 (**F**, H-2)	99.0	C-1 of residue **F**				

542

Table 3. (*Continued*)

Residues	δ_H	Observed connections					
		HMBC		TOCSY		ROESY	
		δ_C	Atom (sequence)	δ_H	Atom	δ_H	Atom
α-Ara*f*-(1→	5.15 (**G**, H-1)	86.8	C-4 of residue **G**				
→5)-α-Ara*f*-(1→	5.09 (**H**, H-1)	85.2	C-4 of residue **H**				
→3,5)-α-Ara*f*-(1→	5.11 (**I**, H-1)	**68.7**	**C-5 of residue H**				
→2)-α-Rha*p*-(1→	1.28 (**J**, H-6)	72.0	C-5 of residue **J**	3.81	H-5 of residue **J**		
		74.8	C-4 of residue **J**	3.47	H-4 of residue **J**		
	1.30 (**J**, H-6)	71.8	C-5 of residue **J**	3.83	H-5 of residue **J**		
		75.1	C-4 of residue **J**				
→2,4)-α-Rha*p*-(1→	1.39 (**K**, H-6)	71.0	C-5 of residue **K**				
→4)-β-Glc*p*-(1→	4.48 (**L**, H-1)			3.36	H-2 of residue **L**		

3.3 SMAP-1 ameliorates DSS-induced colitis in mice

3.3.1 SMAP-1 reduced DSS-induced colon injuries of colitis mice

To evaluate the protective effect of SMAP-1 on colitis, the body weight and DAI of mice were monitored and recorded daily during the DSS intervention. No irregular symptom was observed in the NC group throughout the experiment **(Fig. 3)**. However, the body weight of mice in the DSS group gradually decreased from the 4th day after the DSS intervention (11th day in **Fig. 3B,** $p < 0.05$), and diarrhea, bloody stool, a bent waist, piloerection, and the decreased of food intake and activity were also observed in these mice. These symptoms were slightly ameliorated in SMAP-1 treated mice compared to the DSS group, but no significant difference was observed ($p > 0.05$). DAI scores that reflect clinical symptoms and the severity of the UC mice model increased significantly in the DSS group compared to the NC group from the 11th day ($p < 0.05$), the same as symptoms observed previously (Chassaing et al., 2014). DAI scores of mice treated with different dosages of SMAP-1 all decreased significantly compared to the DSS group (**Fig. 3C**). At the same time, the colon was shortened and the ratio of colonic weight to the length was increased significantly in the DSS group. However, these changes in the colon were noticeably attenuated by SMAP-1 ($p < 0.01$, **Fig. 3D**, **E**, and **F**), even though SMAP-1 had no significant recovery effect on the weight loss caused by DSS (**Fig. 3B**).

DSS has been reported to have a toxic effect on the colonic epithelium and induces erosions that ultimately compromise barrier integrity, resulting in increased colonic epithelial permeability. This further allows the dissemination of pro-inflammatory intestinal contents into the underlying tissues and destroys the balance between innate immunity and gut microbiota (Chassaing et al., 2014). In this study, the intestinal glands and histiocytes in the mucosal layer of mice were seriously damaged after the DSS challenge, and the number of crypt and goblet cells was significantly reduced, as shown in **Fig. 3G-b**. Abscess foci, connective tissue hyperplasia, and a large number of

inflammatory cells (mainly macrophages and neutrophils) infiltrations were observed and have invaded the submucous layer and muscle layer (**Fig. 3G-b**). HAI score of the DSS group was significantly higher than that of the NC group (**Fig. 3H**, $p< 0.001$). In comparison, the inflammatory cell infiltration was lower in SMAP-1 groups than in the DSS group, and a more complete colonic structure, higher numbers of goblet cells, and a relatively more integrated mucosal structure were observed (**Fig. 3G-c, d, e)**. Accordingly, a lower HAI score was shown in all SMAP-1 groups compared to the DSS group (**Fig. 3H**, $p< 0.001$). All results indicated that SMAP-1 ameliorated colitis symptoms and colonic injuries caused by DSS, and might be able to restore the intestinal barrier and reduce colonic inflammation, which would be studied in the following sections.

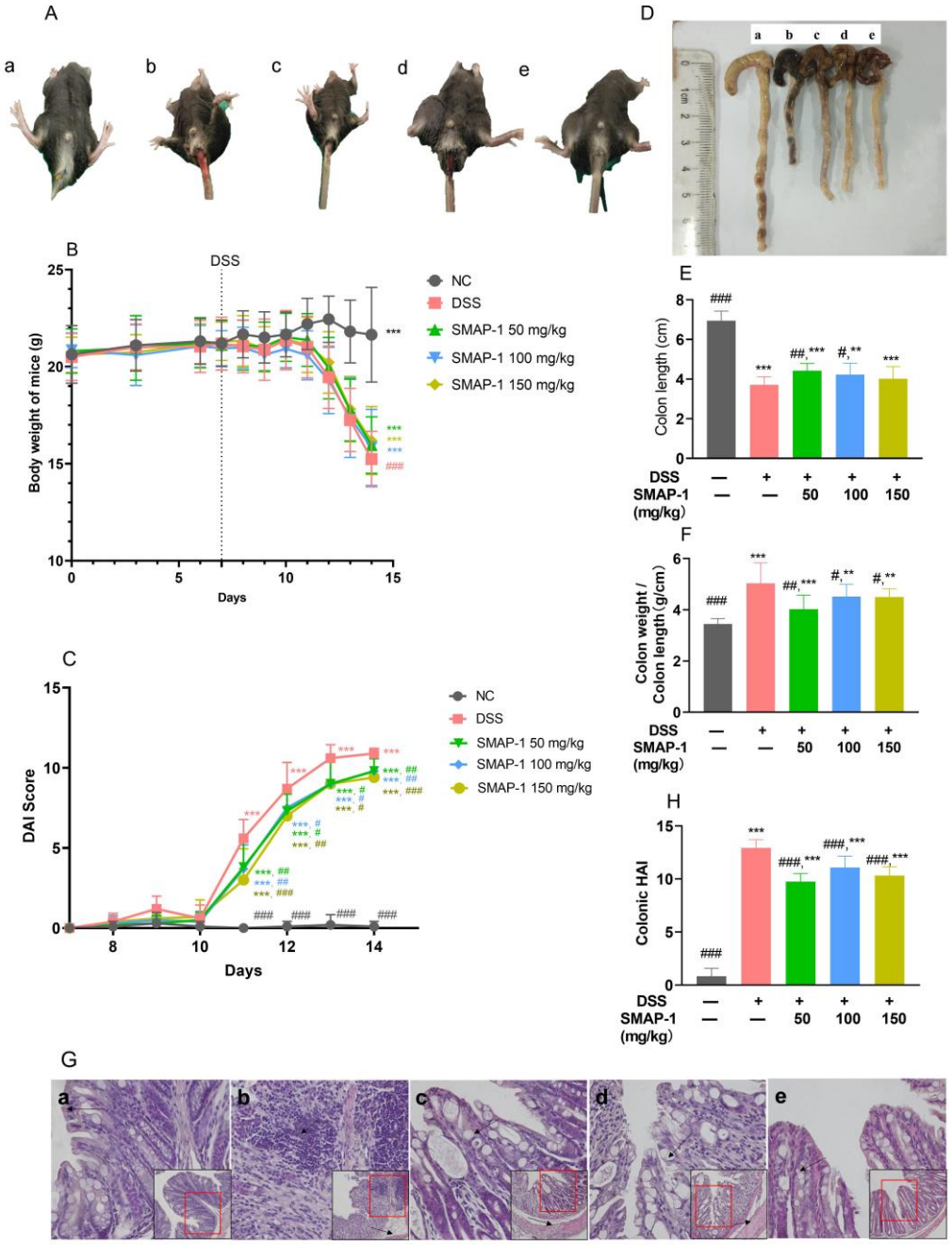

584

585 **Fig. 3.** Effects of SMAP-1 on DSS-induced colitis mice. (A), bloody stool; (B), body weight; (C)
586 DAI score; (D), (E), and (F), colonic damages and shortening; (G), histological damages; (H), HAI
587 score of colonic tissues: (a) NC group, (b) DSS group, (c) 50 mg/kg SMAP-1 group, (d) 100 mg/kg
588 SMAP-1 group, (e) 150 mg/kg SMAP-1 group. Data were shown as the mean ± SD. * $p < 0.05$, **
589 $p < 0.01$, and *** $p < 0.001$ compared to NC group; # $p < 0.05$, ## $p < 0.01$, and ### $p < 0.001$
590 compared to DSS group.

3.3.2 SMAP-1 reduced DSS-induced colonic inflammation of colitis mice

MPO has been shown to be a local mediator of tissue damage and results in inflammation in various inflammatory diseases (Aratani, 2018). As shown in **Fig. 4A**, the content of colonic MPO in the DSS group was statistically higher than in the NC group ($p < 0.001$). In addition, excessive secretion of pro-inflammatory cytokines as inflammatory indicators, including IL-1β, IL-6, and TNF-α, has been reported to lead to the development of inflammation in IBD patients (Akdis et al., 2016). The levels of these cytokines were significantly increased in the colon of DSS-induced colitis mice, but were further reduced significantly in all SMAP-1 treated groups (**Fig. 4B, C**, and **D**). The levels of an anti-inflammatory interleukin, IL-10, and an important inflammatory mediator, TGF-β (Akdis et al., 2016), were both reduced by DSS treatment and restored by SMAP-1 (**Fig. 4E** and **F**). The combination of pro-inflammatory and anti-inflammatory cytokines is a key indicator for understanding the inflammatory status of intestinal defense (Y. Wang et al., 2019), which suggested that, in the current study, DSS induced a disorder between pro-inflammatory and anti-inflammatory cytokines in the colon. While, SMAP-1 could regulate such imbalance and relieve colitis, as many plant-derived polysaccharides have exhibited in previous studies (Wang, Li, Zha, & Luo, 2022).

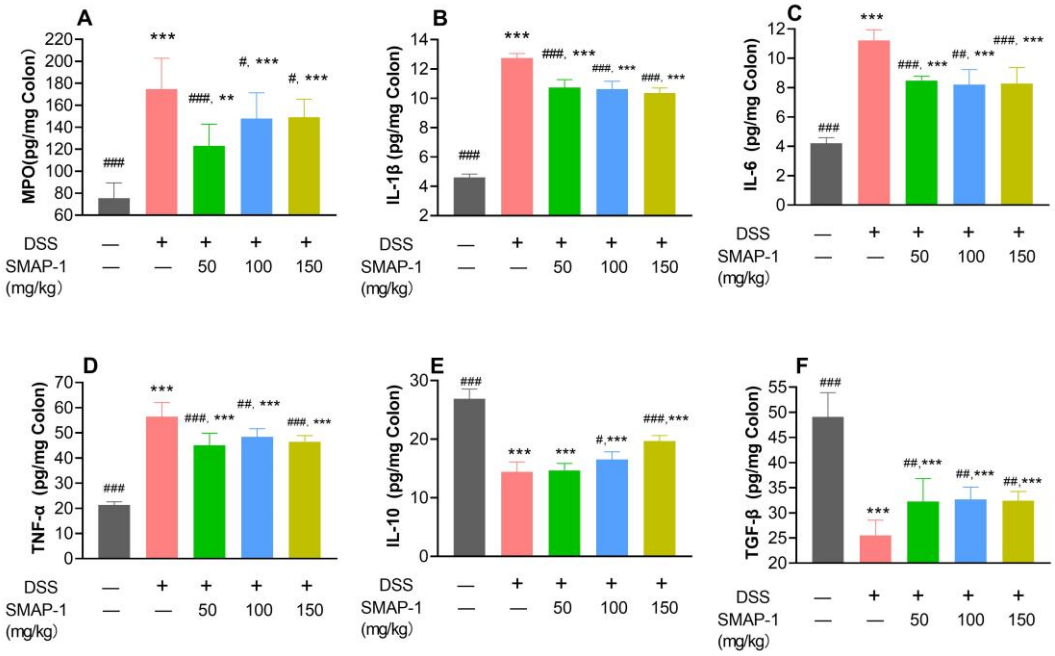

Fig. 4. Effects of SMAP-1 on colonic inflammation of DSS-induced colitis mice. (A), MPO, (B), IL-1β, (C), IL-6, (D), TNF-α, (E), IL-10, (F), TGF-β; * $p < 0.05$, ** $p < 0.01$, and *** $p < 0.01$ compared to NC group; # $p < 0.05$, ## $p < 0.01$, and ### $p < 0.001$ compared to DSS group.

3.3.3 SMAP-1 promoted antioxidant defense of colitis mice by activating Nrf2 signaling pathway

It has been reported that oxidative stress is a crucial factor to induce and aggravate inflammation in the intestine, as the intestinal tract is a vulnerable site to oxidative stress in the existence of harsh environmental factors. High productions of oxidative stress-related molecules, like ROS, MPO, and MDA, are further triggered (Bourgonje et al., 2020; Yuan, Li, Huang, Fu, & Dong, 2022). While, a variety of plant-derived polysaccharides possess antioxidative activities, and they are effective in the treatment of experimental IBD or UC by ameliorating oxidative stress (Wang et al., 2022; Yuan et al., 2022). This also applied to SMAP-1. As shown in **Fig. 5**, statistically lower levels of GSH-PX and SOD, and a higher level of MDA in both colon and serum of colitis mice were observed compared to the NC group. Nevertheless, those in SMAP-1-treated

mice were oppositely regulated in a dose-dependent manner compared to the colitis mice.

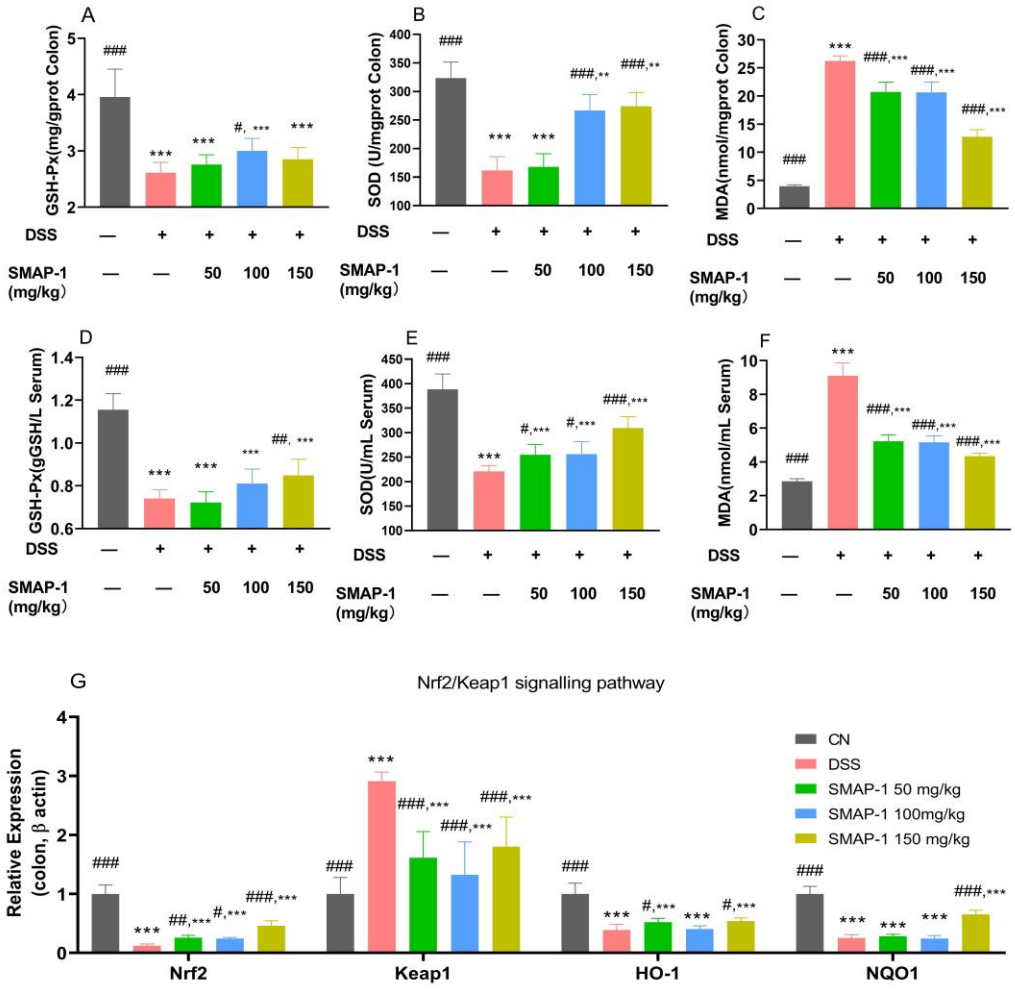

Fig. 5. Effects of SMAP-1 on oxidative status and Nrf2 signal pathway of DSS-induced colitis mice. The levels of oxidative stress were represented by the contents of GSH-Px (A), SOD (B), and MDA (C) in serum, and the contents of GSH-Px (D), SOD (E), and MDA(F) in the colon. *, $p < 0.05$, **, $p < 0.01$, and ***, $p < 0.01$ compared to NC group; #, $p< 0.05$, ##, $p< 0.01$, and ###, $p < 0.001$ compared to DSS group.

The anti-oxidant efficiency of SMAP-1 could be achieved through the regulation of Nrf2 signaling pathway as we hypothesized in the introduction. As shown in **Fig. 5G**, the gene transcriptions of Nrf2 and its downstream genes, HO-1 and NQO1, were significantly down-regulated by the DSS intervention compared to the NC group, while,

the gene transcription of Keap1 was dramatically upregulated. However, these gene transcriptions were significantly reversed by SMAP-1 ($p < 0.05$). Moderate effects were observed on the modulation of HO-1 by 100 mg/kg SMAP-1, and NQO1 by 50 and 100 mg/kg SMAP-1 (**Fig. 5G**, $p > 0.05$). Collectively, the high-dosage of SMAP-1 performed the best effect in the regulation of Nrf2 signaling pathway. These findings suggested that SMAP-1 could play a beneficial role in DSS-induced colitis through anti-oxidative effects by activating Nrf2 signaling pathway. Similar effects of other plant-derived polysaccharides have been reported previously (Chen et al., 2021; Yuan et al., 2019). The mechanism of the modulatory effect of SMAP-1 on this signaling pathway could be proposed that SMAP-1 inhibits the connection between Keap1 and Nrf2, or promotes the expression and translocation of Nrf2. The up-regulation of Nrf2 and its translocation to the nucleus further activate the expressions of stress-responsive protein and/or ROS scavenging enzymes (including HO-1, GSH-PX, and SOD) in the cell nucleus to eliminate excessive ROS. However, xenobiotics detoxification represented by NQO1 enzyme may not be involved (Piotrowska et al., 2021).

3.3.4 SMAP-1 repaired the integrity of the intestinal barrier

Damage to the intestinal mucosal barrier is another important factor associated with IBD (Guan, 2019). And as mentioned previously, it has been shown that the main reason why DSS induces colitis in mice is the destruction of intestinal barrier function (Chassaing et al., 2014). Mucins secreted by intestinal goblet cells form a barrier that prevents large particles, including most bacteria, from directly contacting the epithelial cell layer. And the apical junctional complex, which is composed of the tight and subjacent adherence junction ensures an intact intestinal epithelial layer (Turner, 2009). Here, the increased level of LPS in serum suggested that the barrier in the colonic layer of colitis mice was damaged by DSS intervention (**Fig. 6A**). And the gene expressions of mucin 2 (Muc 2), a peripheral membrane protein ZO-1, a transmembrane protein claudin 4 and a transmembrane tight junction protein occludin, were all downregulated

by DSS, as shown in **Fig. 6B, C, D,** and **E**, respectively ($p < 0.001$). This indicates that DSS led to the destruction of the intestinal barrier in colitis mice. SMAP-1 reduced the level of LPS in serum and upregulated the gene expression of Muc-2, ZO-1, claudin 4, and occludin in the colon. These results suggest that SMAP-1 could restore the intestinal barrier function of colitis mice. This restorative effect on barrier defense could be due to the inhibition of intestinal inflammation and/or the reduction of oxidative stress observed by SMAP-1 in the above sections, as correlations among them have already been reported (Bourgonje et al., 2020; Turner, 2009). Up-regulation of Nrf2 has also been shown to strengthen tight junctions in the intestinal epithelium (Piotrowska et al., 2021). Regulation of intestinal microbiota composition is another potential factor, similar to the previously reported effects of a variety of polysaccharides (Yuan et al., 2022).

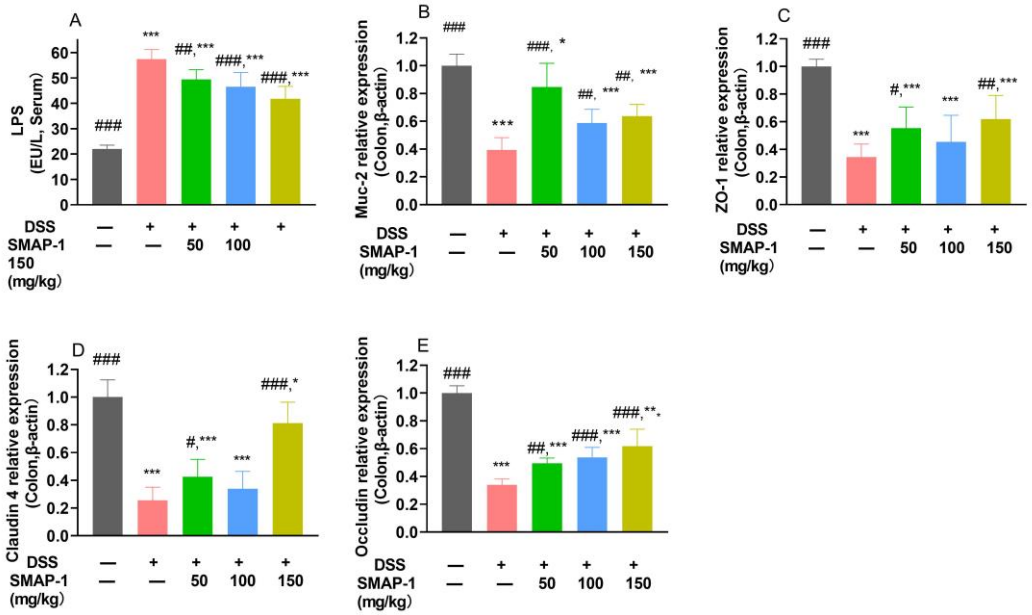

Fig. 6. Effect of SMAP-1 on intestinal epithelial barrier function in colitis mice. (A), the content of LPS in serum; the relative gene expression levels of Muc-2 (B), ZO-1(C), claudin 4 (D), and occludin (E). *, $p < 0.05$, **, $p < 0.01$, and ***, $p < 0.001$ compared to NC group; #, $p< 0.05$, ##, $p< 0.01$, and ###, $p< 0.001$ compared to DSS group.

3.3.5 SMAP-1 modulated the serum metabolomic profiles of DSS-induced colitis mice

Metabolomics is an analysis of the profile of small-molecule intermediates and end products in biological samples. The metabolomic profile of serum and plasma, the most commonly studied biofluids, can well-characterize biological profiles and reflect systemic metabolism. Metabolomic analysis in IBD could provide information on disease-associated metabolic changes and may reflect changes in host metabolism over time and following therapeutic interventions (Gallagher, Catesson, Griffin, Holmes, & Williams, 2021). In this study, untargeted metabolomics of mice serum was used to investigate the modulatory effect of SMAP-1 on the metabolite profiles of DSS-induced colitis. Three randomly mixed samples were tested for data quality control (QC) before starting the analysis. The Pearson correlation of the QC samples is shown in **Fig. S3.** The higher the correlation of the QC samples (R^2 was closer to 1), the more stable the whole detection process and the higher the data quality. There were 469 (negative mode) and 656 (positive mode) known metabolites detected and identified in all NC, DSS, and SMAP-1 (150 mg/kg) groups. Furthermore, a principal component analysis (PCA, **Fig. 7A, B**) and a partial least squares discriminant analysis (PLS-DA, **Fig. 7C**, **D**) were used to investigate the similarity of the principal components and the overall metabolic differences among samples of each group. The difference between the NC (control) and DSS (model) groups was not that apparent, however, the metabolomic profile of the SMAP-1-treated group was independently distributed from the other two groups **(Fig. 7A-D)**, indicating that the serum metabolite profile of the colitis mice was changed after SMAP-1 intervention.

Differential metabolites between groups that matched with VIP > 1.0, FC > 1.5, or FC < 0.667 and P value < 0.05, were further screened. There were 113 and 90 metabolites found in the positive and negative mode, respectively. Herein, 30 metabolites in the positive mode and 18 metabolites in the negative mode were

significantly modulated in the DSS group compared to the NC group (**Table S4**). While, after the treatment of SMAP-1, 66 metabolites in the positive mode and 50 metabolites in the negative mode were regulated compared to the DSS group, as shown in **Table S5**. These altered metabolites in all three groups were independently distributed in PCA and PLS-DA analysis **(Fig. 7E-H)**. Of all the aforementioned metabolites, 9 metabolites that were upregulated in the DSS group, were downregulated by SMAP-1. While, 15 metabolites that were downregulated in the DSS group, were upregulated by SMAP-1, as shown in the heatmaps in **Fig. 8A, B,** and the details in **Fig. S4**.

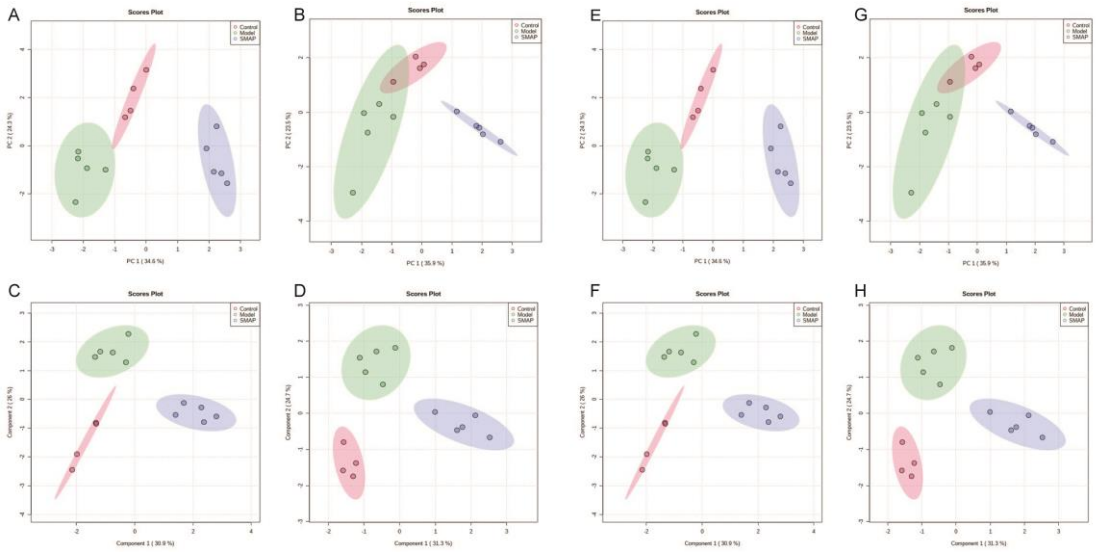

Fig. 7. Effects of SMAP-1 on the overall (A-D) and differential metabolites (E-H) of DSS-induced colitis mice. (A, E), PCA in the positive mode; (B, F), PCA in the negative mode; (C, G), PLS-DA in the positive mode; (D, H), PLS-DA in the negative mode.

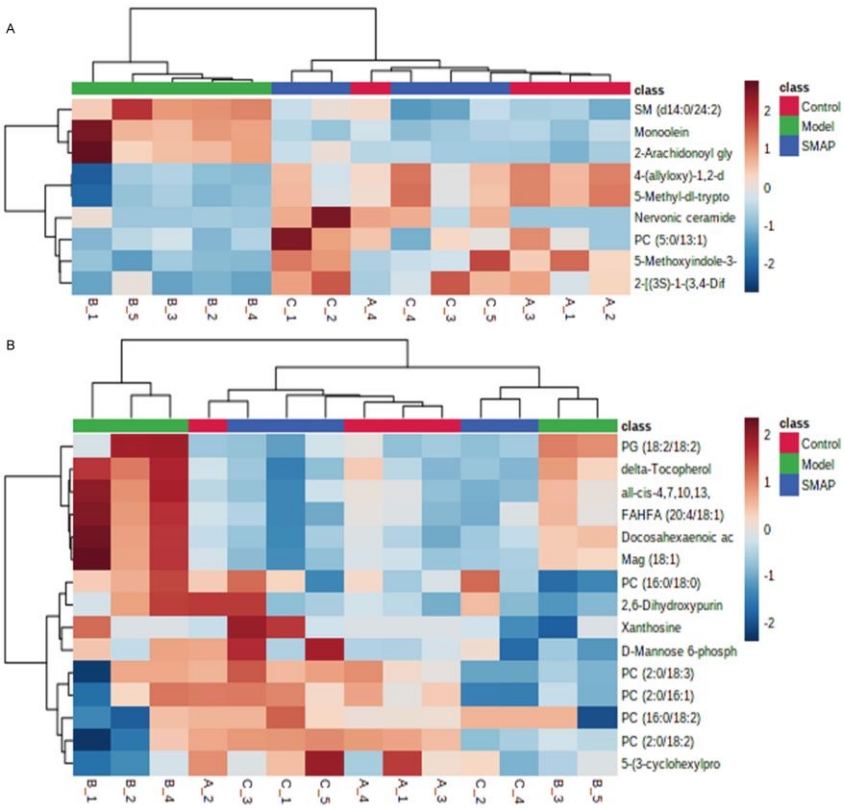

Fig. 8. Cluster heatmaps of metabolites that were reversed by SMAP-1 on DSS-induced colitis mice in positive (A) and negative modes (B).

Furthermore, a spearman correlation was performed to analyze the correlations between the regulated metabolites mentioned in this section and the levels of MPO, cytokines (IL-1β, TNF-α, IL-6, IL-10, TGF-β), and antioxidant-related enzymes (GSH-PX, SOD, and MDA) shown in earlier sections. As shown in **Fig. 9**, the serum metabolites that were extremely altered by treatment with DSS and SMAP-1 were screened. Seven of them showed significant correlations with the modulatory effects of SMAP-1 on cytokines and antioxidatant enzymes. To date, numerous studies have investigated the effects of the metabolites docosahexaenoic acid (DHA), 2-arachidonoyl, glycerol, xanthine, and docosapentaenoic acid on colitis by reducing intestinal inflammatory factors in colitis or IBD (Chiaro et al., 2017; Perisetti, Rimu, Khan, Bansal, & Goyal, 2020; Wu et al., 2020; Zhao et al., 2017b; Zheng, Dai, Cao,

Shen, & Zhang, 2019). However, the potential effect of 5-methoxy indole-3-carboxaldehyde (5-MC), which has been shown to corelate significantly with the anti-inflammatory and anti-oxidative effects observed by SMAP-1, on colitis remains unknown and was therefore chosen for further investigation.

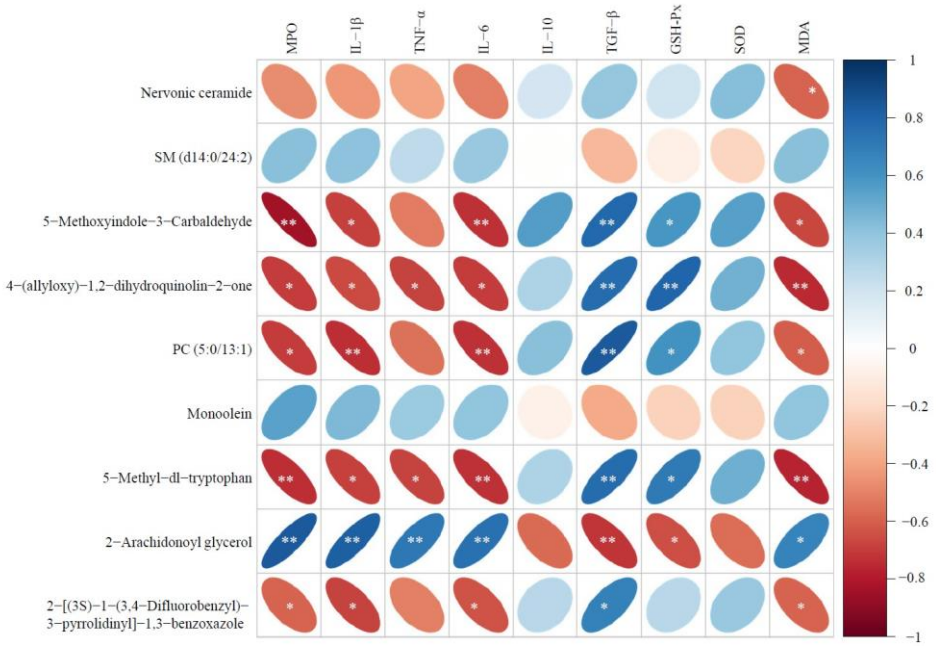

Fig. 9. Spearman correlations between the levels of pro-inflammatory cytokines and oxidative stress-related proteins and the identified metabolites in serum. */**, represents the correlation was statistically significant, * $p<0.05$, ** $p<0.01$.

3.4 Effects of SMAP-1 and 5-methoxy indole-3-carbaldehyde on the LPS-induced IPEC-J2 cells

To further confirm the anti-oxidative effects of SMAP-1 *in vitro* through its modulatory potential on Nrf2/Keap1 signaling pathway, SMAP-1 was administered to inflamed intestinal epithelial cells (IPEC-J2). Additionally, 5-MC, the metabolite significantly regulated by SMAP-1 *in vivo*, was also studied to determine its effects on the inflamed intestinal epithelium and whether it is one of the major targets that SMAP-1 affected *in vivo*. LPS has been used to induce inflammation and oxidative stress on

IPEC-J2 cells, as has been previously reported (Z.-G. Chen et al., 2018; Huang et al., 2021; Zou et al., 2020). The cytotoxicity of SMAP-1, 5-MC, and LPS was initially tested using CCK-8 kits. All these three compounds were shown to be nontoxic on IPEC-J2 cells in the range of 1.25 or 5 to 20 μg/mL (**Fig. 10A**). 10 and 20 μg/mL of 5-MC promoted cell proliferation after 12 h co-cultivation (**Fig. 10A**). Therefore, 20 μg/mL LPS and 5, 10, and 20 μg/mL SMAP-1 and 5-MC were used in further studies.

As shown in **Fig. 10,** both gene and protein expressions of antioxidant enzymes (CAT, SOD, GSH-Px) were downregulated in the LPS-treated group compared to the normal control. They were, however, significantly restored in dose-dependent manners after pretreatment with SMAP-1 (**Fig. 10B, a-f**) and 5-MC (**Fig. 10C, a-f**). This suggests that both SMAP-1 and 5-MC could promote protection against cellular oxidation in IPEC-J2 cells. These modulatory effects of SMAP-1 were consistent with those observed in colitis mice. In addition, Nrf2/Keap1 signaling pathway which had been regulated *in vivo* was also activated by SMAP-1 *in vitro.* Gene transcription levels of Nrf2 and its relevant proteins NQO1 and HO-1 were upregulated, and that of Keap1 was downregulated by SMAP-1, being consistent with the effects observed in DSS-induced colitis mice in section 3.3.3. Moreover, SMAP-1 was characterized as a pectic polysaccharide in section 3.2, and its protective effects against oxidative stress on LPS-induced IPEC-J2 cells were similar to those of other pectic polysaccharides shown previously (Huang et al., 2021; Zou et al., 2021; Zou et al., 2020; Zou et al., 2022), by enhancing the activities of antioxidant enzymes and activating Nrf2/Keap1 signaling pathway. Interestingly, both 5-MC and SMAP-1 were effective in regulating Nrf2/Keap1 signaling pathway in a dose-dependent manner. As far as we know, 5-MC is a synthesized compound and has not yet been isolated from nature (Jeyaseelan, Premkumar, Kaviyarasu, & Franklin Benial, 2019). Few biological functions have been studied besides its anti-lung cancer potential. Its anti-oxidative ability on the intestine is the first report. At the same time, the level of 5-MC was dramatically decreased in

colitis mice and promoted by SMAP-1 treatment (**Fig. S4**). It might be one of the end products of SMAP-1 after oral administration, and also a metabolite from specific bacteria that could be affected by SMAP-1. Further study invovling human bacteria/feces could be of interest to investigate the source of 5-MC and degradation of SMAP-1 the by gut microbiota. It is possible that SMAP-1 exerts its protective effect on colitis mice by regulating the amount of 5-MC in the colon, and that 5-MC could be further absorbed into the blood and continues to function in the circulatory system. Therefore, 5-MC could be one of the signals/compounds that are derived from and controlled by SMAP-1 *in vivo*. An *in vivo* study of 5-MC in colitis mice with dynamic monitoring of 5-MC levels in both colonic contents and serum would be helpful to verify this hypothesis. Further evidence on the relationship between 5-MC and colitis or IBD is needed. In conclusion, this study demonstrated robust protective effects of a pectic polysaccharide isolated from the aerial parts of *S. miltiorrhiza* on colitis and the intestinal epithelium and provided a foundation for the future utilization of these wasted aerial plant parts. Additionally, 5-MC could be a potential candidate and the target signaling metabolite for the action of SMAP-1 to defend against intestinal oxidative stress in colitis through Nrf2/Keap1, which needs to be further investigated.

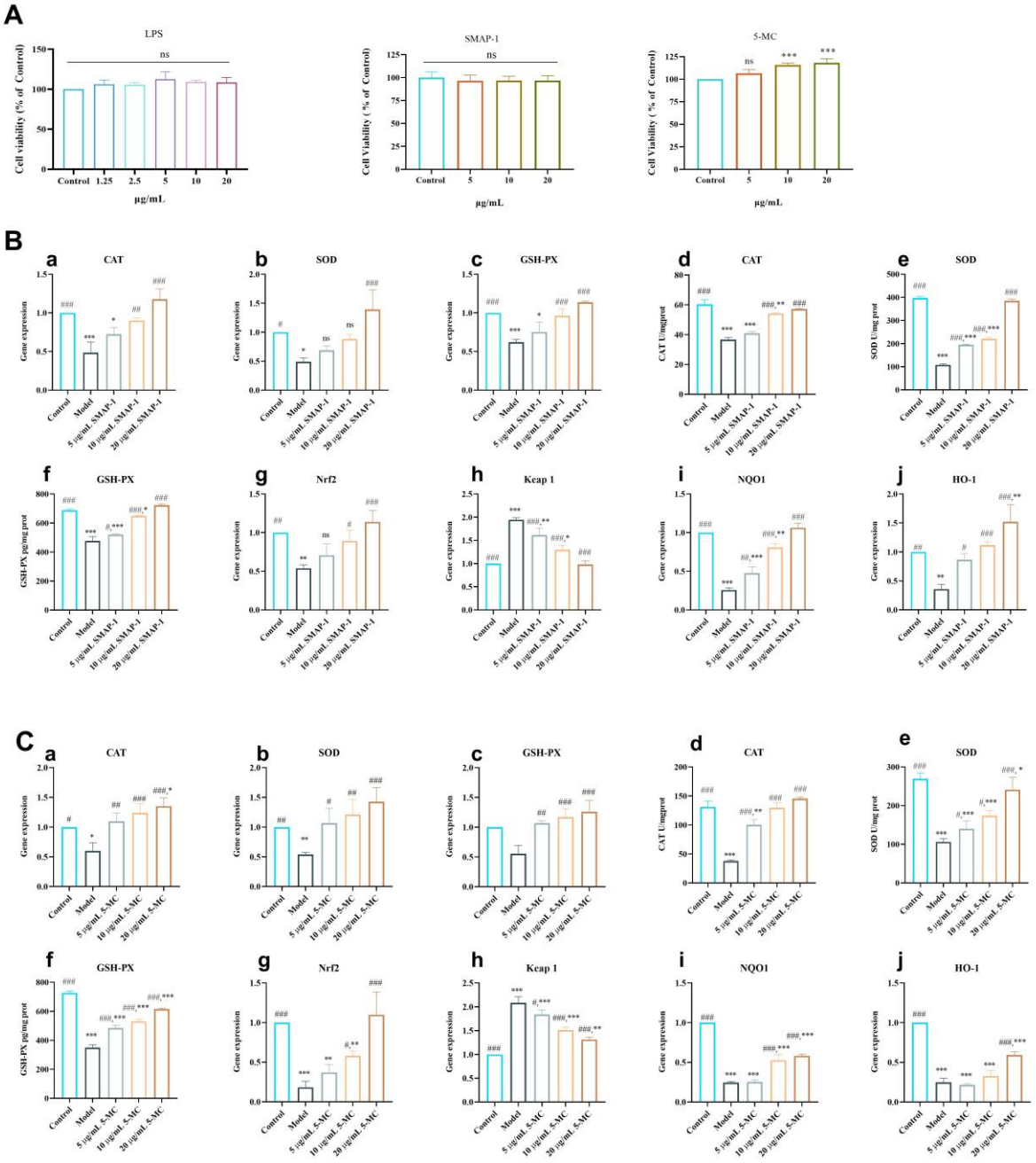

Fig. 10. Cell viability and antioxidant effects of SMAP-1 and 5-MC on IPEC-J2 cells. Cells were pretreated with SMAP-1 or 5-MC at 5, 10, and 20 μg/mL for 12 h before supplemented with LPS (20 μg/mL). (A), cell viability of cells treated with LPS, SMAP-1, and 5-MC; (B), gene and protein expressions of CAT (a, d), SOD (b, e), and GSH-PX (c, f), as well as gene expressions of Nrf2 (g), Keap1 (h), NQO1 (i) and HO-1 (j) in cells treated with SMAP-1; (C), gene and protein expressions of CAT (a, d), SOD (b, e) and GSH-PX (c, f), as well as gene expressions of Nrf2 (g), Keap1 (h), NQO1 (i) and HO-1 (j) in cells treated with 5-MC. * p<0.05, ** p<0.01, *** p<0.001 vs. Control group; # p<0.05, ## p<0.01, ### p<0.001 vs. Model/LPS only group; ns, no significant difference.

4 Conclusion

In this study, a pectic polysaccharide, SMAP-1, with 26.3 kDa and consisting of HG and RG-I regions with arabinans and possible AG-I and AG-II side chains, was isolated from the aerial part of *S. miltiorrhiza*. SMAP-1 exhibited robust protective effects on DSS-induced colitis by activating Nrf2/Keap1 signaling pathway. In addition, SMAP-1 reversed the levels of several metabolites that were affected by DSS. The metabolite 5-MC also exhibited anti-oxidative effects by regulating Nrf2/Keap1 signaling pathway *in vitro*, same as SMAP-1 performed. These results suggested that SMAP-1 could be a promising candidate for the treatment of colitis, and 5-MC could be the signal metabolite for the action of SMAP-1 in defending against intestinal oxidative stress in colitis. This study also laid the foundation for further utilization of the wasted aerial parts of *S. miltiorrhiza* as a medicinal sources of antioxidant substance.

Acknowledgment

This work was supported in part by the Program Sichuan Veterinary Medicine and Drug Innovation Group of China Agricultural Research System (SCCXTD-2020-18). It was also partly supported by the Research Council of Norway through the Norwegian NMR Platform, NNP (226244/F50). We acknowledged the support of Key Laboratory of Animal Disease and Human Health of Sichuan Province.

CRediT Authorship contribution statement

Yu-Ping Fu: Data curation, Visualization; Writing – review & editing. **Xi Peng**: Data curation, Methodology Visualization Investigation, Software, Writing. **Chao-Wen Zhang:** Data curation, Methodology Visualization Investigation, Software, Writing. **Quan-Xing Jiang**: Data curation, Methodology, Software. **Cen-Yu Li**: Methodology,

Visualization, Formal analysis, Software. **Berit Smestad Paulsen**: Methodology, Writing – review & editing. **Frode Rise**: Data curation. **Chao Huang**: Methodology, Supervision. **Bin Feng**: Supervision. **Li-Xia Li**: Investigation. **Xing-Fu Chen**: Software. **Ren-Yong Jia**: Supervision. **Yang-Ping Li**: Investigation. **Xing-Hong Zhao**: Writing – review & editing. **Gang Ye**: Visualization. **Hua-Qiao Tang**: Methodology. **Xiao-Xia Liang**: Formal analysis. **Cheng Lv**: Supervision; Visualization. **Meng-Liang Tian**: Visualization. **Zhong-Qiong Yin**: Funding acquisition, Project administration Writing–review & editing. **Yuan-Feng Zou**: Funding acquisition, Project administration, Resources, Data curation, Methodology, Roles/Writing - original draft.

References:

Ahmad, M. M., Chatha, S. A. S., Iqbal, Y., Hussain, A. I., Khan, I., & Xie, F. (2022). Recent trends in extraction, purification, and antioxidant activity evaluation of plant leave-extracted polysaccharides. *Biofuels, Bioprod. Bioref., 16*, 1820-1848. https://doi.org/10.1002/bbb.2405

Akdis, M., Aab, A., Altunbulakli, C., Azkur, K., Costa, R. A., Crameri, R., Duan, S., Eiwegger, T., Eljaszewicz, A., Ferstl, R., Frei, R., Garbani, M., Globinska, A., Hess, L., Huitema, C., Kubo, T., Komlosi, Z., Konieczna, P., Kovacs, N., Kucuksezer, U. C., Meyer, N., Morita, H., Olzhausen, J., O'Mahony, L., Pezer, M., Prati, M., Rebane, A., Rhyner, C., Rinaldi, A., Sokolowska, M., Stanic, B., Sugita, K., Treis, A., & d, W. v. (2016). Interleukins (from IL-1 to IL-38), interferons, transforming growth factor β, and TNF-α: Receptors, functions, and roles in diseases. *J. Allergy Clin. Immunol., 138*(4), 984-1010. https://doi.org/10.1016/j.jaci.2016.06.033

Aratani, Y. (2018). Myeloperoxidase: Its role for host defense, inflammation, and neutrophil function. *Arch. Biochem. Biophys., 640*, 47-52. https://doi.org/10.1016/j.abb.2018.01.004

Bernstein, C. N., Fried, M., Krabshuis, J. H., Cohen, H., Eliakim, R., Fedail, S., Gearry, R., Goh, K. L., Hamid, S., Khan, A. G., LeMair, A. W., Malfertheiner, P., Ouyang, Q., Rey, J.-F., Sood, A., Steinwurz, F., Thomsen, O. Ø., Thomson, A., & Watermeyer, G. (2010). World Gastroenterology

Organisation Global Guideline: Inflammatory bowel disease: a global perspective - June 2009. *South Afr. Gastroenterol. Rev.*, *8*(2), 13-23.

Bourgonje, A. R., Feelisch, M., Faber, K. N., Pasch, A., Dijkstra, G., & van Goor, H. (2020). Oxidative stress and redox-modulating therapeutics in inflammatory bowel disease. *Trends Mol. Med.*, *26*(11), 1034-1046. https://doi.org/10.1016/j.molmed.2020.06.006

Bradford, M.-M. (1976). A rapid and sensitive method for the quantitation of microgram quantities of protein utilizing the principle of protein-dye binding. *Anal. Biochem.*, *72*, 248-254. https://doi.org/10.1006/abio.1976.9999

Chambers, R. E., & Clamp, J. R. (1971). An assessment of methanolysis and other factors used in the analysis of carbohydrate-containing materials. *Biochem. J.*, *125*, 1009-1018. https://doi.org/10.1042/bj1251009

Chassaing, B., Aitken, J. D., Malleshappa, M., & Vijay-Kumar, M. (2014). Dextran sulfate sodium (DSS)-induced colitis in mice. *Curr. Prot. Immunol.*, *104*, 15.25.11-15.25.14. https://doi.org/10.1002/0471142735.im1525s104

Chen, Y., Hu, J., Zhang, Y., Han, C., & Li, J. (2018). Anti-Alzheimer's disease effect of essential oil from aerial parts of *Salvia miltiorrhiza* Bge. *Int. J. Clin. Exp. Med.*, *11*(2), 641-652.

Chen, Y., Wang, J., Li, J., Zhu, J., Wang, R., Xi, Q., Hongya, W., Tongguo, S., & Weichang, C. (2021). Astragalus polysaccharide prevents ferroptosis in a murine model of experimental colitis and human Caco-2 cells via inhibiting NRF2/HO-1 pathway. *Eur. J. Pharmacol.*, *911*, 174518. https://doi.org/10.1016/j.ejphar.2021.174518

Chen, Z.-G., Yuan, Q.-L., Xu, G.-R., Chen, H.-Y., Lei, H.-Y., & Su, J.-M. (2018). Effects of quercetin on proliferation and H_2O_2-induced apoptosis of intestinal porcine enterocyte cells. *Molecules*, *23*(8), 2012. https://doi.org/10.3390/molecules23082012

Chiaro, T. R., Soto, R., Stephens, W. Z., Kubinak, J. L., Petersen, C., Gogokhia, L., Bell, R., Delgado, J. C., Cox, J., Voth, W., Brown, J., Stillman, D. J., O'Connell, R. M., Tebo, A. E., & Round, J. L. (2017). A member of the gut mycobiota modulates host purine metabolism exacerbating colitis in mice. *Sci. Transl. Med.*, *9*(380), eaaf9044. http://doi.org/9044.10.1126/scitranslmed.aaf9044

Chylińska, M., Szymańska-Chargot, M., & Zdunek, A. (2016). FT-IR and FT-Raman characterization of non-cellulosic polysaccharides fractions isolated from plant cell wall. *Carbihydr. Polym.*, *154*, 48-54. https://doi.org/10.1016/j.carbpol.2016.07.121

Ciucanu, I., & Kerek, F. (1984). A simple and rapid method for the permethylation of carbohydrates. *Carbohydr. Res.*, *131*(2), 209-217. https://doi.org/10.1016/0008-6215(84)85242-8

900 Dénou, A., Togola, A., Inngjerdingen, K. T., Moussavi, N., Rise, F., Zou, Y. F.,
901 Dafam, D. G., Nep, E. I., Ahmed, A., Alemika, T. E., Diallo, D., Sanogo, R.,
902 & Paulsen, B. S. (2022). Isolation, characterisation and complement fixation
903 activity of acidic polysaccharides from *Argemone mexicana* used as
904 antimalarials in Mali. *Pharm. Biol.*, *60*(1), 1278-1285.
905 https://doi.org/10.1080/13880209.2022.2089691
906 Dubois, M., Gilles, K. A., Hamilton, J. K., Rebers, P. A., & Smith, F. (1956).
907 Colorimetric method for determination of sugars and related substances. *Anal.*
908 *Chem.*, *28*(3), 350-356. https://doi.org/https://doi.org/10.1021/ac60111a017
909 Gallagher, K., Catesson, A., Griffin, J. L., Holmes, E., & Williams, H. R. T. (2021).
910 Metabolomic analysis in inflammatory bowel disease: A systematic review. *J.*
911 *Crohns Colitis*, *15*(5), 813-826. https://doi.org/10.1093/ecco-jcc/jjaa227
912 Guan, Q. (2019). A comprehensive review and update on the pathogenesis of
913 inflammatory bowel disease. *J. Immunol. Res.*, *2019*, 7247238.
914 https://doi.org/10.1155/2019/7247238
915 Hao, D. C., Ge, G. B., & Xiao, P. G. (2018). Anticancer drug targets of Salvia
916 phytometabolites: Chemistry, biology and omics. *Curr. Drug Targets*, *19*(1),
917 1-20. https://doi.org/10.2174/1389450117666161207141020
918 Huang, C., Peng, X., Pang, D.-J., J. L., Paulsen, B.-S., Rise, F., Chen, Y.-L., Z.-L. C.,
919 Jia, R.-Y., Li, L.-X., Song, X., Feng, B., Z.-Q. Y., & Zou, Y.-F. (2021). Pectic
920 polysaccharide from *Nelumbo nucifera* leaves promotes intestinal antioxidant
921 defense *in vitro* and *in vivo*. *Food Funct.*, *12*(21), 10828-10841.
922 https://doi.org/10.1039/d1fo02354c
923 Hwang, J., Jin, J., Jeon, S., Moon, S. H., Park, M. Y., Yum, D. Y., Kim, J. H., Kang,
924 J. E., Park, M. H., Kim, E. J., Pan, J. G., Kwon, O., & Oh, G. T. (2020). SOD1
925 suppresses pro-inflammatory immune responses by protecting against
926 oxidative stress in colitis. *Redox. Biol.*, *37*, 101760.
927 https://doi.org/10.1016/j.redox.2020.101760
928 Jeyaseelan, S. C., Premkumar, R., Kaviyarasu, K., & Franklin Benial, A. M. (2019).
929 Spectroscopic, quantum chemical, molecular docking and *in vitro* anticancer
930 activity studies on 5-Methoxyindole-3-carboxaldehyde. *J. Molecul. Struct.*,
931 *1197*, 134-146. https://doi.org/10.1016/j.molstruc.2019.07.042
932 Jia, Z. Y., Xu, C. F., Shen, J. Q., Xia, T. L., Yang, J. F., & He, Y. (2015). The natural
933 compound celastrol inhibits necroptosis and alleviates ulcerative colitis in
934 mice. *Int. Immunopharmacol.*, *29*(2), 552-559.
935 https://doi.org/10.1016/j.intimp.2015.09.029
936 Jiang, Y. Y., Li, Y. B., Yu, J., Chen, H., Zhou, J., Wang, L., Zhang, L., Zhao, M. J.,
937 Zhou, Y. H., & Yu, L. (2020). Preliminary structure and bioactivities of
938 polysaccharide SMWP-U&E isolated from *Salvia miltiorrhiza* Bunge residue.
939 *Int. J. Biol. Macromol.*, *157*, 434-443.
940 https://doi.org/10.1016/j.ijbiomac.2020.04.092

Jing, Y., Hu, J., Su, Z., Cheng, W., Zhang, Y., Yang, X., Zhang, D., & Wu, L. (2022). Structural characterisation and antioxidant activities *in vitro* and *in vivo* of a novel polysaccharide from *Salvia miltiorrhiza*. *Nat. Prod. Res.*, 1-6. https://doi.org/10.1080/14786419.2022.2096605

Kaczmarska, A., Pieczywek, P. M., Cybulska, J., & Zdunek, A. (2022). Structure and functionality of Rhamnogalacturonan I in the cell wall and in solution: A review. *Carbohydr. Polym.*, *278*, 118909. https://doi.org/10.1016/j.carbpol.2021.118909

Kim, J.-B., & Carpita, N.-C. (1992). Changes in esterification of the uronic acid groups of cell wall polysaccharides during elongation of maize coleoptiles. *Plant Physiol.y*, *98*(2), 646-653. https://doi.org/10.1104/pp.98.2.646

Komalavilas, P., & Mort, A. J. (1989). The acetylation of O-3 of galacturonic acid in the rhamnose-rich portion of pectins. *Carbohydr. Res.*, *189*, 261-272. https://doi.org/10.1016/0008-6215(89)84102-3

Kostálová, Z., Hromádková, Z., & Ebringerová, A. (2013). Structural diversity of pectins isolated from the Styrian oil-pumpkin (*Cucurbita pepo* var. *styriaca*) fruit. *Carbohydr. Polym.*, *93*, 163-171. https://doi.org/10.1016/j.carbpol.2012.05.017

Kpodo, F. M., Agbenorhevi, J. K., Alba, K., Bingham, R. J., Oduro, I. N., Morris, G. A., & Kontogiorgos, V. (2017). Pectin isolation and characterization from six okra genotypes. *Food Hydrocolloids*, *72*, 323-330. https://doi.org/10.1016/j.foodhyd.2017.06.014

Kyomugasho, C., Christiaens, S., Shpigelman, A., Van-Loey, A.-M., & Hendrickx, M.-E. (2015). FT-IR spectroscopy, a reliable method for routine analysis of the degree of methylesterification of pectin in different fruit- and vegetable-based matrices. *Food Chem.*, *176*(1), 82-90. https://doi.org/10.1016/j.foodchem.2014.12.033

Lee, S. H., Kwon, J. E., & Cho, M. L. (2018). Immunological pathogenesis of inflammatory bowel disease. *Intest. Res.*, *16*(1), 26-42. https://doi.org/10.5217/ir.2018.16.1.26

Li, M. Z., Zhong, Z., & Moses, S. S. C. (2005). Danshen: An overview of its chemistry, pharmacology, pharmacokinetics, and clinical use. *J. Clin. Pharmacol.*, *45*(12), 1345-1359. https://doi.org/10.1177/0091270005282630

Li, P., Xiao, N., Zeng, L.-P., Xiao, J., Huang, J.-z., Xu, Y.-n., Chen, Y.-L., Ren, Y.-H., & Du, B. (2020). Structural characteristics of a mannoglucan isolated from Chinese yam and its treatment effects against gut microbiota dysbiosis and DSS-induced colitis in mice. *Carbohydr. Polym.*, *250*, 116958. https://doi.org/10.1016/j.carbpol.2020.116958

Li, S.-S., Yang, G., Yan, J.-M., Wu, D., Hou, Y., Diao, Q.-Y., & Zhou, Y.-F. (2018). Polysaccharide structure and immunological relationships of RG-I pectin from

the bee pollen of *Nelumbo nucifera*. *Int. J. Biol. Macromol., 111*, 660-666. https://doi.org/10.1016/j.ijbiomac.2018.01.015

Li, X., Chen, Q., Liu, G., Xu, H., & Zhang, X. (2021). Chemical elucidation of an arabinogalactan from rhizome of *Polygonatum sibiricum* with antioxidant activities. *Int. J. Biol. Macromol., 190*, 730-738. https://doi.org/10.1016/j.ijbiomac.2021.09.038

Li, Z. M., Xu, S. W., & Liu, P. Q. (2018). Salvia miltiorrhizaBurge (Danshen): a golden herbal medicine in cardiovascular therapeutics. *Acta Pharmacol. Sinica, 39*(5), 802-824. https://doi.org/10.1038/aps.2017.193

Luo, S., Shu, H. Y., & Chen, X. B. (2019). Experiment and modeling of seated hunan body exposed to large-magnitude vibration in six single directions *J. Mech. Med. Biol., 19*(5), 217-227. https://doi.org/10.1142/s0219519419500374

Mehta, S. J., Lindsay, J. O., & Silver, A. R. (2013). Review article: Strategies for the management of chronic unremitting ulcerative colitis. *Aliment. Pharmacol. Ther., 38*(2), 77-97. https://doi.org/10.1111/apt.12345

Mohnen, D. (2008). Pectin structure and biosynthesis. *Curr. Opin. Plant Biol., 11*(3), 266-277. https://doi.org/10.1016/j.pbi.2008.03.006

Nyman, A. A. T., Aachmann, F. L., Rise, F., Ballance, S., & Samuelsen, A. B. C. (2016). Structural characterization of a branched (1 → 6)-a-mannan and b-glucans isolated from the fruiting bodies of *Cantharellus cibarius*. *Carbohydr. Polym., 146*, 197-207. https://doi.org/10.1016/j.carbpol.2016.03.052

Patova, O. A., Smirnov, V. V., Golovchenko, V. V., Vityazev, F. V., Shashkov, A. S., & Popov, S. V. (2019). Structural, rheological and antioxidant properties of pectins from *Equisetum arvense* L. and *Equisetum sylvaticum* L. *Carbohydr. Polym., 209*, 239-249. https://doi.org/10.1016/j.carbpol.2018.12.098

Perisetti, A., Rimu, A. H., Khan, S. A., Bansal, P., & Goyal, H. (2020). Role of cannabis in inflammatory bowel diseases. *Ann. Gaastroenterol., 33*(2), 134-144. https://doi.org/10.20524/aog.2020.0452

Pettolino, F.-A., Walsh, C., Fincher, G.-B., & Bacic, A. (2012). Determining the polysaccharide composition of plant cell walls. *Nat. Prot., 7*(9), 1590-1607. https://doi.org/10.1038/nprot.2012.081

Piotrowska, M., Swierczynski, M., Fichna, J., & Piechota-Polanczyk, A. (2021). The Nrf2 in the pathophysiology of the intestine: Molecular mechanisms and therapeutic implications for inflammatory bowel diseases. *Pharmacol. Res., 163*, 105243. https://doi.org/10.1016/j.phrs.2020.105243

Rosenbohm, C., Lundt, I., Christensen, T. I. E., & Young, N. G. (2003). Chemically methylated and reduced pectins: preparation, characterisation by ^{1}H NMR spectroscopy, enzymatic degradation, and gelling properties. *Carbohydr. Res., 338*(7), 637-649. https://doi.org/10.1016/s0008-6215(02)00440-8

Shakhmatov, E.-G., Atukmaev, K.-V., & Makarova, E.-N. (2016). Structural characteristics of pectic polysaccharides and arabinogalactan proteins from

Heracleum sosnowskyi Manden. *Carbohydr. Polym.*, *136*, 1358-1369. https://doi.org/10.1016/j.carbpol.2015.10.041

Shakhmatov, E.-G., Belyy, V.-A., & Makarova, E.-N. (2018). Structure of acid-extractable polysaccharides of tree greenery of *Picea abies*. *Carbohydr. Polym.*, *199*, 320-330. https://doi.org/10.1016/j.carbpol.2018.07.027

Shakhmatov, E. G., Makarova, E. N., & Belyy, V. A. (2019). Structural studies of biologically active pectin-containing polysaccharides of pomegranate *Punica granatum*. *Int. J. Biol. Macromol.*, *122*, 29-36. https://doi.org/10.1016/j.ijbiomac.2018.10.146

Singleton, V. L., & Rossi, J. A. (1965). Colorimetry of total phenolics with phosphomolybdic-phosphotungstic acid reagent. *Am. J. Enol. Vitic.*, *16*, 144-158 https://www.ajevonline.org/content/16/3/144

Sweet, D. P., Shapiro, R. H., & Albersheim, P. (1975). Quantitative analysis by various g.l.c. response-factor theories for partially methylated and partially ethylated alditol acetates. *Carbohydr. Res.*, *40*(2), 217-225. https://doi.org/10.1016/S0008-6215(00)82604-X

Tahvilian, N., Masoodi, M., Faghihi Kashani, A., Vafa, M., Aryaeian, N., Heydarian, A., Hosseini, A., Moradi, N., & Farsi, F. (2021). Effects of saffron supplementation on oxidative/antioxidant status and severity of disease in ulcerative colitis patients: A randomized, double-blind, placebo-controlled study. *Phytother. Res.*, *35*(2), 946-953. https://doi.org/10.1002/ptr.6848

Tu, W., Wang, H., Li, S., Liu, Q., & Sha, H. (2019). The anti-Inflammatory and anti-oxidant mechanisms of the Keap1/Nrf2/ARE signaling pathway in chronic diseases. *Aging Dis.*, *10*(3), 637-651. https://doi.org/10.14336/AD.2018.0513

Turner, J. R. (2009). Intestinal mucosal barrier function in health and disease. *Nat. Rev. Immunol.*, *9*(11), 799-809. https://doi.org/10.1038/nri2653

Varki, A., Cummings, R.-D., Aebi, M., Packer, N.-H., Seeberger, P.-H., Esko, J.-D., Stanley, P., Hart, G., Darvill, A., Kinoshita, T., Prestegard, J.-J., Schnaar, R.-L., Freeze, H.-H., Marth, J.-D., Bertozzi, C.-R., Etzler, M.-E., Frank, M., Vliegenthart, J.-F.-G., Tteke, T., & Perez, S. (2015). Symbol Nomenclature for Graphical Representations of Glycans. *Glycobiology*, *25*(12), 1323-1324. https://doi.org/10.1093/glycob/cwv091

Wang, X., Han, C., Qin, J., Wei, Y., Qian, X., Bao, Y., & Shi, W. (2019). Pretreatment with *Salvia miltiorrhiza* polysaccharides protects from lipopolysaccharides/D-galactosamine-Iinduced liver injury in mice through inhibiting TLR4/MyD88 signaling pathway. *J. Interferon Cytokine Res.*, *39*(8), 495-505. https://doi.org/10.1089/jir.2018.0137

Wang, Y.-J., Li, Q.-M., Zha, X.-Q., & Luo, J.-P. (2022). Intervention and potential mechanism of non-starch polysaccharides from natural resources on ulcerative colitis: A review. *Int. J. Biol. Macromol*., *210*, 545-564 https://doi.org/10.1016/j.ijbiomac.2022.04.208

Wang, Y., Zhang, N., Kan, J., Zhang, X., Wu, X., Sun, R., Tang, S., Liu, J., Qian, C., & Jin, C. (2019). Structural characterization of water-soluble polysaccharide from Arctium lappa and its effects on colitis mice. *Carbohydr. Polym., 213*, 89-99. https://doi.org/10.1016/j.carbpol.2019.02.090

Wang, Y. L., Zhang, Q., Yin, S. J., Cai, L., Yang, Y. X., Liu, W. J., Hu, Y.-J., Chen, H., & Yang, F.-Q. (2018). Screening of blood-activating active components from Danshen-Honghua herbal pair by spectrum-effect relationship analysis. *Phytomedicine, 54*, 149-158. https://doi.org/10.1016/j.phymed.2018.09.176

Wen, Z., Liu, W., Li, X., Chen, W., Liu, Z., Wen, J., & Liu, Z. (2019). A protective role of the NRF2-Keap1 pathway in maintaining intestinal barrier function. *Oxid. Med. Cell Longev., 2019*, 1759149. https://doi.org/10.1155/2019/1759149

Wold, C. W., Kjeldsen, C., Corthay, A., Rise, F., Christensend, B. E., Duusb, J. Ø., & Inngjerdingen, K. T. (2018). Structural characterization of bioactive heteropolysaccharides from the medicinal fungus *Inonotus obliquus* (Chaga). *Carbohydr. Polym., 185*, 27-40. https://doi.org/10.1016/j.carbpol.2017.12.041

Wu, J., Wei, Z., Cheng, P., Qian, C., Xu, F., Yang, Y., Wang, A., Chen, W., Sun, Z., & Lu, Y. (2020). Rhein modulates host purine metabolism in intestine through gut microbiota and ameliorates experimental colitis. *Theranostics, 10*(23), 10665-10679. http://doi.org/10.7150/thno.43528

Xiang, X. (2019). Study on the Bio-active Components and Mechanism of the Stems and Leaves of *Salvia miltiorrhiza* on Diabetic Renal Injury. Naijing University of Chinese Medicine, Nanjing, China.

Yang, F., Wi, Y., & Zhang, Y. (2020). Research progress on chemical constituents and pharmacological effects of aerial parts of *Salvia miltiorrhiza*. *Chin. Trad. Patent Med., 42*(6), 1558-1564. https://doi.org/10.3969/j.issn.100l-1528.2020.06.032

Yang, W., Zhao, P., Li, X., Guo, L., & Gao, W. (2022). The potential roles of natural plant polysaccharides in inflammatory bowel disease: A review. *Carbohydr. Polym., 277*, 118821. https://doi.org/10.1016/j.carbpol.2021.118821

Yao, H.-Y.-Y., Wang, J.-Q., Yin, J.-Y., Nie, S.-P., & Xie, M.-Y. (2021). A review of NMR analysis in polysaccharide structure and conformation: Progress, challenge and perspective. *Food Res. Int., 143*, 110290. https://doi.org/10.1016/j.foodres.2021.110290

Yu, C., Yu, J., Gu, J., Su, S., Hua, Y., & Duan, J. (2018). Effect and mechanism of aerial parts of Salvia miltiorrhiza effective constituents on glycolipid metabolism of high sugar-induced Drosophila melanogaster metabolic disorder model. *Chin. J. Chin. Materia Med., 43*(7), 1484-1491

Yuan, D., Li, C., Huang, Q., Fu, X., & Dong, H. (2022). Current advances in the anti-inflammatory effects and mechanisms of natural polysaccharides. *Crit. Rev. Food Sci. Nutr.*, 1-21. https://doi.org/10.1080/10408398.2022.2025535

Yuan, Z., Yang, L., Zhang, X., Peng, C., Yongli, H., & Yanming, W. (2019). Huang-Lian-Jie-Du decoction ameliorates acute ulcerative colitis in mice via regulating NF-κB and Nrf2 signaling pathways and enhancing intestinal barrier function, *Front. Pharmacol.*, *10*, 1354. https://doi.org/10.3389/fphar.2019.01354

Zaitseva, O., Khudyakov, A., Sergushkina, M., Solomina, O., & Polezhaeva, T. (2020). Pectins as a universal medicine. *Fitoterapia, 146*, 104676. https://doi.org/10.1016/j.fitote.2020.104676

Zeng, H.-T., Su, S.-L., Xiang, X., Sha, X.-X., Zhu, Z.-H., Wang, Y.-Y., Guo, S., Yan, H., Qian, D.-W., & Duan, J.-A. (2017). Comparative analysis of the major chemical constituents in *Salvia miltiorrhiza* roots, stems, leaves and flowers during different growth periods by UPLC-TQ-MS/MS and HPLC-ELSD methods. *Molecules, 22*(5), 771. https://doi.org/10.3390/molecules22050771

Zhao, J., Dong, J.-N., Wang, H.-G., Zhao, M.-L., Sun, J., Zhu, W.-M., Zuo, L.-G., Gong, J.-F., Li, Y., Gu, L. L., Li, N., & Li, J.-S. (2017). Docosahexaenoic acid attenuated experimental chronic colitis in interleukin 10–deficient mice by enhancing autophagy through inhibition of the mTOR pathway. *J. Parenteral Enteral Nutr., 41*(5), 824-829. https://doi.org/10.1177/0148607115609308

Zhao, K., Li, B., He, D., Zhao, C., Shi, Z., Dong, B., Pan, D., Patil, R. R., Yan, Z., & Guo, Z. (2020). Chemical characteristic and bioactivity of hemicellulose-based polysaccharides isolated from *Salvia miltiorrhiza*. *Int. J. Biol. Macromol., 165*(Pt B), 2475-2483. https://doi.org/10.1016/j.ijbiomac.2020.10.113

Zheng, Z., Dai, Z., Cao, Y., Shen, Q., & Zhang, Y. (2019). Docosapentaenoic acid (DPA, 22:5n-3) ameliorates inflammation in an ulcerative colitis model. *Food Funct., 10*(7), 4199-4209. http://doi.org/10.1039/C8FO02338G

Zou, Y.-F., Chen, M.-S., Fu, Y.-P., Zhu, Z.-K., Zhang, Y.-Y., Paulsen, B.-S., Rise, F., Chen, Y.-L., Yang, Y.-Z., Jia, R.-Y., Li, L.-X., Song, X., Tang, H.-Q., Feng, B., Lv, C., Ye, G., Wu, D.-T., Yin, Z.-Q., & Huang, C. (2021). Characterization of an antioxidant pectic polysaccharide from *Platycodon grandiflorus*. *Int. J. Biol. Macromol., 175*, 473-480. https://doi.org/10.1016/j.ijbiomac.2021.02.041

Zou, Y.-F., Chen, X.-F., Malterud, K.-E., Rise, F., Barsett, H., Inngjerdingen, K.-T., Michaelsen, T.-E., & Paulsen, B.-S. (2014). Structural features and complement fixing activity of polysaccharides from *Codonopsis pilosula* Nannf. var. *modesta* L.T.Shen roots. *Carbohydr, Polym., 113*(26), 420-429. https://doi.org/10.1016/j.carbpol.2014.07.036

Zou, Y.-F., Fu, Y.-P., Chen, X.-F., Austarheim, I., Inngjerdingen, K. T., Huang, C., Lei, F.-Y., Song, X., Li, L., Ye, G., Eticha, L. D., Yin, Z., & Paulsen, B. S. (2017). Polysaccharides with immunomodulating activity from roots of *Gentiana crassicaulis*. *Carbohydr. Polym., 172*, 306-314. https://doi.org/10.1016/j.carbpol.2017.04.049

Zou, Y.-F., Zhang, Y.-Y., Paulsen, B.-S., Rise, F., Chen, Z.-L., Jia, R.-Y., Li, L.-X., Song, X., Feng, B., Tang, H.-Q., Huang, C., & Yin, Z.-Q. (2020). Structural features of pectic polysaccharides from stems of two species of Radix Codonopsis and their antioxidant activities. *Int. J. Biol. Macromol., 159*, 704-713. https://doi.org/10.1016/j.ijbiomac.2020.05.083

Zou, Y. F., Li, C. Y., Fu, Y. P., Jiang, Q. X., Peng, X., Li, L. X., Song, X., Zhao, X. H., Li, Y. P., Chen, X. F., Feng, B., Huang, C., Jia, R. Y., Ye, G., Tang, H. Q., & Yin, Z. Q. (2022). The comparison of preliminary structure and intestinal anti-inflammatory and anti-oxidative activities of polysaccharides from different root parts of *Angelica sinensis* (Oliv.) Diels. *J. Ethnopharmacol., 295*, 115446. https://doi.org/10.1016/j.jep.2022.115446